MATERIALS CHEMISTRY FRONTIERS

REVIEW

View Article Online
View Journal

Cite this: DOI: 10.1039/d3qm00828b

Materials design and applications of n-type and ambipolar organic electrochemical transistors

Yuqiu Lei,[b] Peiyun Li,[a] Yuting Zheng[b] and Ting Lei *[a]

Received 25th July 2023,
Accepted 7th September 2023

DOI: 10.1039/d3qm00828b

rsc.li/frontiers-materials

Organic electrochemical transistors (OECTs) have high transconductance, low operating voltages, and good biocompatibility. They have emerged as a promising technology for chemo/biosensors, bioelectronics, neuromorphic computing, *etc.* Compared with the abundant high-performance p-type OECT materials, n-type and ambipolar OECT materials are rare and, more importantly, their performances lag far behind, which largely limited the development of OECT-based logic circuits. The past few years have witnessed the fast development of n-type and ambipolar OECT materials and their applications, thanks to the efforts of novel materials design and device optimization. In this review, we aim to provide an introduction to the working principles of n-type and ambipolar OECTs and survey their recent developments and applications. We will also discuss the challenges and issues that need to be addressed for the future advancement of the field.

1 Introduction

Organic semiconductors are organic materials that can switch between insulating and conducting states.[1] The switching process involves a change in charge carrier concentration, leading to electron or hole transport. Such control over charge carrier transport can be achieved through field-effect, chemical, and or electrochemical doping methods.[2] Organic electrochemical transistors (OECTs), utilizing organic semiconductors as channels, can modulate electrical signals by interacting directly with the electrolyte through electrochemical doping,[3] whereas organic field-effect transistors (OFETs) employ field-effect doping to modulate electrical signals, in which the channel materials are in contact with the insulating layer.[4] Compared to OFETs, bulk doping of organic semiconducting layers endows OECTs with high transconductance and low operating voltages. In addition, OECTs can work in aqueous media, exhibiting good biocompatibility, suitable for direct interfacing with biological systems. These features have made OECTs a promising technology for various applications such as chem/biosensing,[5] electrophysiological recording,[6] and neuromorphic computing.[7–9] Complementary logic circuits serve as fundamental building blocks for constructing intricate logic circuits.[10] They provide several benefits such as improved transistor performance (faster switching speed and higher sensitivity), decreased power consumption, enabling the realization of complex functions, and facilitating integration and compatibility with existing electronic devices. Therefore, the development of complementary logic circuits based on

[a] *Key Laboratory of Polymer Chemistry and Physics of Ministry of Education, School of Materials Science and Engineering, Peking University, Beijing 100871, P. R. China. E-mail: tinglei@pku.edu.cn*
[b] *College of Engineering, Peking University, Beijing 100871, P. R. China*

Yuqiu Lei

Yuqiu Lei obtained her BE in optoelectronic information science and engineering from Jinan University in 2021. She is currently pursuing her MS at Peking University. Her research focuses on organic electrochemical transistors and their applications in bioelectronics, as well as the doped nature of organic semiconductor materials.

Peiyun Li

Peiyun Li obtained her BE in materials science from the Huazhong University of Science and Technology in 2019. She is currently pursuing her PhD at Peking University. Her research focuses on organic electrochemical transistors and their applications in flexible electronics, neuromorphic computing, and bioelectronics.

OECTs represents a crucial milestone in the transition from laboratory-based applications to commercial viability.

Depending on the predominant charge carrier types, OECT materials can be categorized as p-type, n-type, or ambipolar. The p-type materials are capable of transporting holes, while the n-type materials primarily transport electrons. An ambipolar material is characterized by its ability to transport both holes and electrons.[11] To date, in contrast to the plentiful high-performance p-type OECT materials, n-type and ambipolar OECT materials are scarce and, more importantly, their performances lag behind by approximately an order of magnitude (as evaluated by μC^*, a performance index in OECTs). This is primarily due to the considerable challenges in the development of n-type materials and the lack of systematic research dedicated to ambipolar materials.[12] The reported p-type OECT material, such as p(g_2T_2-g_4T_2),[13] exhibits a μC^* value exceeding 500 F cm^{-1} V^{-1} s^{-1}. In contrast, the highest reported value for μC^* in n-type materials with operational stability is approximately 50 F cm^{-1} V^{-1} s^{-1}.[14] Moreover, no single-component ambipolar materials with balanced n-type and p-type characteristics have been reported yet.[15] Therefore, the scarcity of high-performance n-type and ambipolar OECT materials severely restricts the development of high-performance complementary logic circuits, which require balanced n-type and p-type OECTs or ambipolar materials with matched n-type and p-type characteristics. In recent years, there has been a growing focus on the application research of n-type materials and ambipolar materials. These include constructing complementary logic circuits,[16–18] enhanced electrophysiological recordings,[19] high-sensitivity electrochemical biosensing,[20–22] and versatile neuromorphic simulation[23] (Fig. 1).

Complementary logic circuits have demonstrated intriguing advantages in enhanced electrophysiological recording,[18] high-sensitivity ion monitoring,[24] and multifunctional neuromorphic simulation.[25] Firstly, these circuits enable advanced real-time, *in situ* monitoring of electrophysiological signals by providing voltage output, surpassing the capabilities of single transistors that solely provide current output. In addition, they significantly improve ion detection accuracy by one to two orders of magnitude, compared to all existing transistors, including single p-type OECTs.[24] Furthermore, significant progress has been made in the field of neuromorphic computing with the successful realization of multifunctional circuits based on complementary logic circuits. It realizes the complete process simulation from synapses to neurons for the first time,[25] while previous development based on p-type transistors was limited to simulating simple synaptic behaviors.[26] Finally, the incorporation of vertical inverter structures[19,27] and the utilization of ambipolar materials yield a 50% reduction in device size, offering valuable insights for integrated processing advancements. In addition to the benefits of constructing complementary logic circuits, n-type OECTs exhibit higher performance in biological sensing, particularly enzyme-based sensing.[28–30] This is due to their capability to stabilize electrons through direct electron transport in the channel. Thus, the construction of complementary logic circuits and the advantages offered by n-type materials in biosensing have been successfully demonstrated, which benefited from the rapid development of n-type and ambipolar materials.

In recent years, notable advancements have been made in developing new n-type OECTs, benefiting from various new design strategies and device optimizations. These advancements include the development of a no-side-chain polymer BBL, the introduction of conductive polymer PBFDO,[31] the proposal of ''doped state engineering'',[14] and the use of small molecule materials.[32,33] Among these materials, PBFDO has shown impressive performance.[31] However, PBFDO possesses a hydrophobic backbone with no hydrophilic side chains and it only shows good performance in thin films ($\sim$50 nm). Moreover, the polymer is intrinsically highly doped in low on/off ratios and we have found that it shows poor stability during on–off cycling. Thus, apart from μC^*, many other polymer properties and device parameters are also important for a good OECT material. The current best performing n-type OECT material, P(gTDPP2FT),[14] achieved through doped state engineering, exhibits a maximum μ of 0.35 cm^2 V^{-1} s^{-1}, and a μC^* value as high as 54.8 F cm^{-1} V^{-1} s^{-1}. While there has been a significant improvement in the performance of n-type OECT materials, with a two-order-of-magnitude enhancement compared to the initially studied materials,[34] further advancements are still

Yuting Zheng

Yuting Zheng is currently pursuing her BS in theoretical and applied mechanics at Peking University. Her research focuses on organic electrochemical transistors and their applications in bioelectronics and sensing.

Ting Lei

Ting Lei received his BS degree in chemistry from Peking University in 2008. He continued his study with Prof. Jian Pei at Peking University and obtained his PhD in 2013. He then obtained a postdoctoral fellowship from Stanford University, where he worked with Prof. Zhenan Bao. He joined Peking University as an Assistant Professor in 2018. His current research interests include organic/polymer functional materials, organic electronics, and bioelectronics.

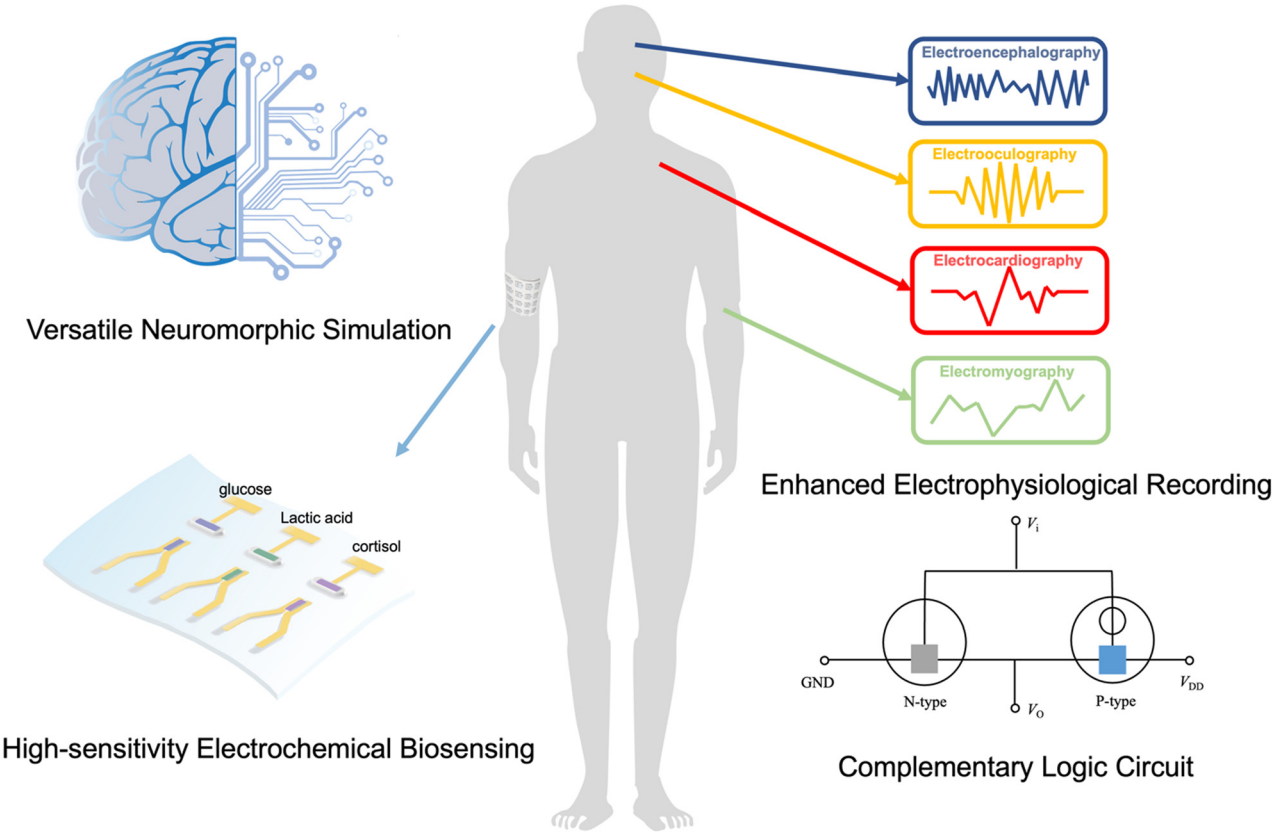

Fig. 1 Applications enabled by high-performance n-type and ambipolar OECTs.

required to match the performance level of existing p-type materials. Furthermore, research on ambipolar materials for OECTs is still in the early stages, which restricts their application in logic circuits with reduced process complexity and device size.[23]

This review aims to explore recent advancements in n-type and ambipolar OECT materials and their applications. Firstly, we will provide an introduction to OECTs, including their operational principles and considerations for device design. Subsequently, we will review the latest advancements in molecular design strategies employed for both n-type and ambipolar OECT materials. We will also discuss various device fabrication techniques that enhance device performance, along with research on improving the stability of n-type materials. Next, we will present an overview of logic circuits based on different material types, emphasizing the importance of developing efficient n-type and ambipolar materials for these circuits. Additionally, we will examine the development and application advantages of complementary logic circuits constructed with n-type or ambipolar materials, as well as the unique benefits that n-type materials offer in the field of biosensing. Finally, we will discuss the prospects and challenges associated with the design and application of n-type and ambipolar materials.

2 Operation principles of OECTs

An OECT is a three-terminal device that consists of a source, a drain, and a gate electrode (Fig. 2a).[35] During OECT operation, a large number of ions in the aqueous electrolyte are directly injected into the active layer by applying a gate bias (V_{GS}), and a change in the carrier concentration modulates the channel current between the source and drain electrodes (I_{DS}). A transistor's sensitivity to voltage modulation is determined by the change of source–drain current, ΔI_{DS}, divided by the change of the applied gate voltage, ΔV_{GS}. The resulting parameter, namely transconductance ($g_m = \partial I_{DS}/\partial V_{GS}$), is a primary figure of merit for a transistor.[36] The most widely used steady-state model in OECTs is the Bernard model.[37] The transconductance, g_m, of an OECT, can be evaluated using eqn (1):

$$g_m = (Wd/L)\mu C^*|(V_{th} - V_{GS})| \quad (1)$$

where W, L, and d are the channel width, length, and thickness, respectively; μ is the charge carrier mobility; C^* is the capacitance per unit volume of the channel; and V_{th} is the threshold voltage. Unlike conventional OFETs that use capacitance per unit area (C_d) of the dielectric layer for calculation, in OECTs, the product dC^* replaces C_d. Therefore, the transconductance of an OECT depends not only on channel geometry (W/L) but also on active layer thickness (d). Due to their volumetric capacitance characteristic, OECTs typically exhibit significantly higher transconductances compared to other transistors. For example, PEDOT:PSS-based p-type OECTs could exhibit high g_m of up to 20 mS,[38] larger than those of graphene transistors and silicon transistors. However, the high transconductance of

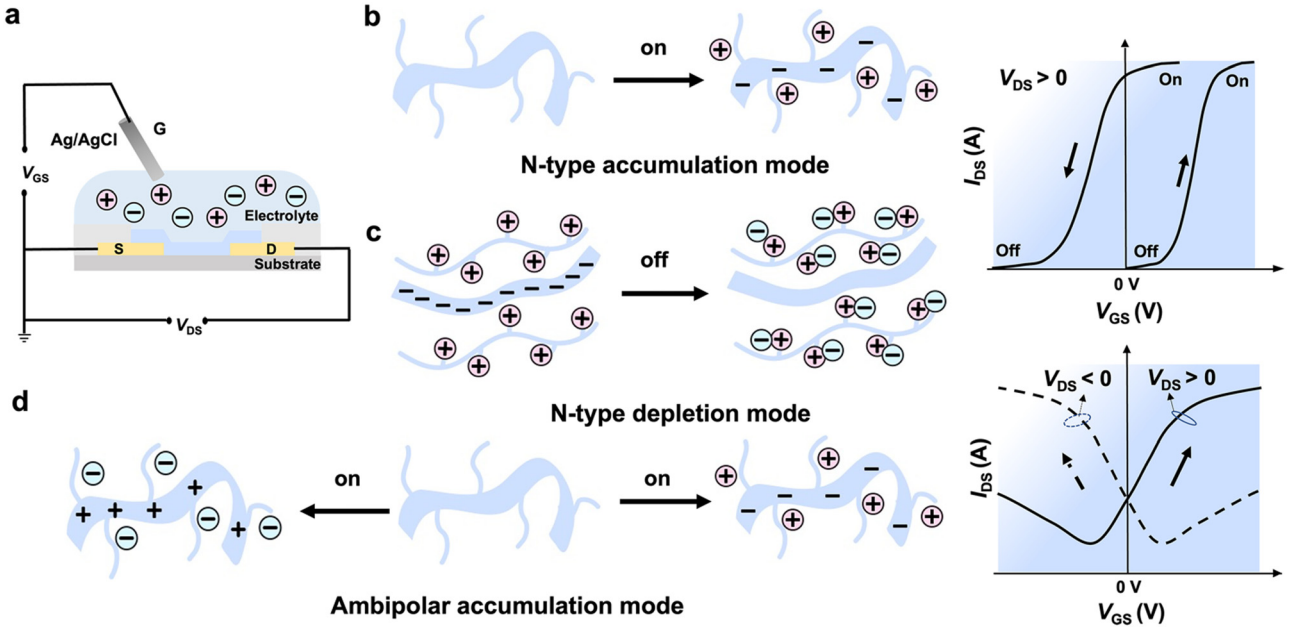

Fig. 2 OECT device structure and operating principle for n-type and ambipolar-based OECTs. (a) Device configuration of an OECT. Operation principle and typical transfer curves of different type and mode OECTs: (b) n-type accumulation mode; (c) n-type depletion mode; and (d) ambipolar accumulation mode.

OECTs comes at the cost of slower response time, which imposes limitations on their maximum response frequency. Based on Bernard's transient model,[37] the change of current with time and V_G is given by eqn (2):

$$I(t, V_{GS}) = I_{ss}(V_{GS}) + [I_{ss}(V_{GS} = 0) - I_{ss}(V_{GS})](1 - g\tau_e/\tau_i)e^{-t/\tau I} \quad (2)$$

where I_{ss} (V_{GS}) is the steady-state source–drain current at a certain gate voltage V_{GS}, g is a fixed geometric factor, τ_e is the electronic transit time, described by $L^2/\mu V_{DS}$, and τ_i is the ionic transit time ($\tau_i = C_G R_S$), which is determined by the electrolyte resistance (R_s) and the capacitance of the ionic double layer (C_G). This model has been proven to be effective in explaining the improvement of response time in the experiments.[39] In this model, the characteristic time constant is determined by the ionic transit time constant τ_i, while the ratio of τ_e to τ_i determines the decaying character. By using the Gouy–Chapman theory,[37] the ionic transit time τ_i can be expressed by $l/c^{1/2}$, where l is the distance between the organic film and gate electrode and c is the ionic concentration. Thus, lowering the l or increasing the c is useful to improve the ionic transit time τ_i. This transient model takes into account the injection of ions from the electrolyte into the channel and the movement of holes within the channel, but it neglects the lateral flow of ions within the channel.

A recently proposed two-dimensional OECT transient model has considered the distribution of ions and holes along the transistor channel to understand the transient behavior of OECTs.[40] The transient response includes two distinct time constants, a short time constant describing the movement of ions perpendicular to the transistor channel and a second, longer one describing the flow of lateral ion currents along the channel, due to the channel length being typically larger than its thickness. Based on this transient model,[40] both increasing the drain voltage (V_{DS}) and decreasing the channel length can accelerate the diffusion of ions, thereby shortening the response time. In addition, this model explains well the reasons for the asymmetry of the on-state and off-state response times. During the transition to the non-conducting state, the dominant mechanism is the longitudinal transport of ions. Conversely, during the transition to the conducting state, ions undergo both longitudinal transport and transverse transport, resulting in a longer transition time to reach the on-state.

The widely used benchmark for the performance comparison of OECT materials is μC^*, where mobility (μ) represents the charge transport ability of the channel material and bulk capacitance (C^*) represents ion permeability.[41,42] However, it is challenging to improve both μ and C^* simultaneously, since enhancing μ by improving molecular packing and structure planarity may hinder ion injection.[43] In the same way, Coulomb interactions can also cause structural and energetic disorders when ions penetrate semiconducting polymers, resulting in impediments to carrier transport.[44,45] Although strategies have been developed to improve ion transport in p-type conjugated polymers, achieving comparable performance for n-type or ambipolar materials remains a challenge.[12] Moreover, accurately characterizing an OECT entails considering additional parameters, such as threshold voltage, an on–off ratio, and stability. The threshold voltage plays a critical role in minimizing Faradaic reactions and conserving power in biosensing applications. Additionally, high on–off ratios contribute to increased sensitivity and signal-to-noise ratios.[46] Furthermore, long-term stability under aqueous conditions is crucial for practical applications. The

evaluation of stability typically involves monitoring the change in drain current (I_D) during a cycle test over the operating voltage range. Additionally, the I_D is monitored over time under constant or pulsed gate voltage bias.[47] These parameters provide valuable insights into the device's performance, stability, and response characteristics, enabling a thorough assessment of its suitability for various applications.

N-Type OECTs can be divided into two operational modes: depletion and accumulation modes.[3] Currently, the majority of reported n-type polymers primarily function in the accumulation mode. In this mode, the device remains inactive with no mobile electrons when the gate voltage is zero. Once a positive gate voltage is applied, cations in the electrolyte permeate into the film, inducing electrons, which increases the drain current and the device reaches an on-state (Fig. 2b). On the other hand, the n-type depletion mode exhibits the opposite behaviour. These materials are inherently doped, which means that they are in the on-state by default. When a negative gate voltage is applied, anions are injected into the channel, neutralizing the electrons and causing the device to transition to the off state (Fig. 2c). Only three reported n-type materials, BBL:PEI,[48] PBFDO[31] (Fig. 3b) and t-gdiPDI[32] (Fig. 5b), work in the depletion mode. Ambipolar materials can transfer both holes and electrons when positive or negative gate voltage is applied, respectively. Notably, the drain current cannot be fully turned off, which is distinct from that of unipolar materials (Fig. 2d).

3 N-Type and ambipolar OECT materials

3.1 Overview of n-type and ambipolar OECT materials

The ion diffusion and doping in OECTs require the hydrophilic nature of the OECT materials.[3] One widely used approach is to utilize hydrophilic oligo(ethylene glycol) (OEG) side chains, as they enhance ion penetration and hydrophilicity in aqueous media. Replacing hydrophobic alkyl chains with hydrophilic side chains has proven to be an effective method for converting OFET materials into OECT materials.[49] Using such an approach, the first ambipolar OECT material p(gNDI-gT2)[34] (Fig. 3c) with stable n-type performance was reported in 2016. While increasing the hydrophilicity of side chains can enhance the bulk capacitance, excessive water absorption can result in irreversible damage to molecular packing,[41,42] leading to reduced electron mobility and poor device stability. Therefore, careful design of the hydrophilic side chain content is necessary. Moreover, the remarkable n-type performance and stability exhibited by BBL,[17] coupled with the introduction of high-performance PBFDO materials,[31] have generated enthusiasm for polymers lacking side chains. However, the main hurdles to their further advancement lie in the intricate chemical structure that is difficult to modify and the harsher processing conditions necessary to address their lower solubility. Except for the polymers, small molecules have also received attention due to their outstanding

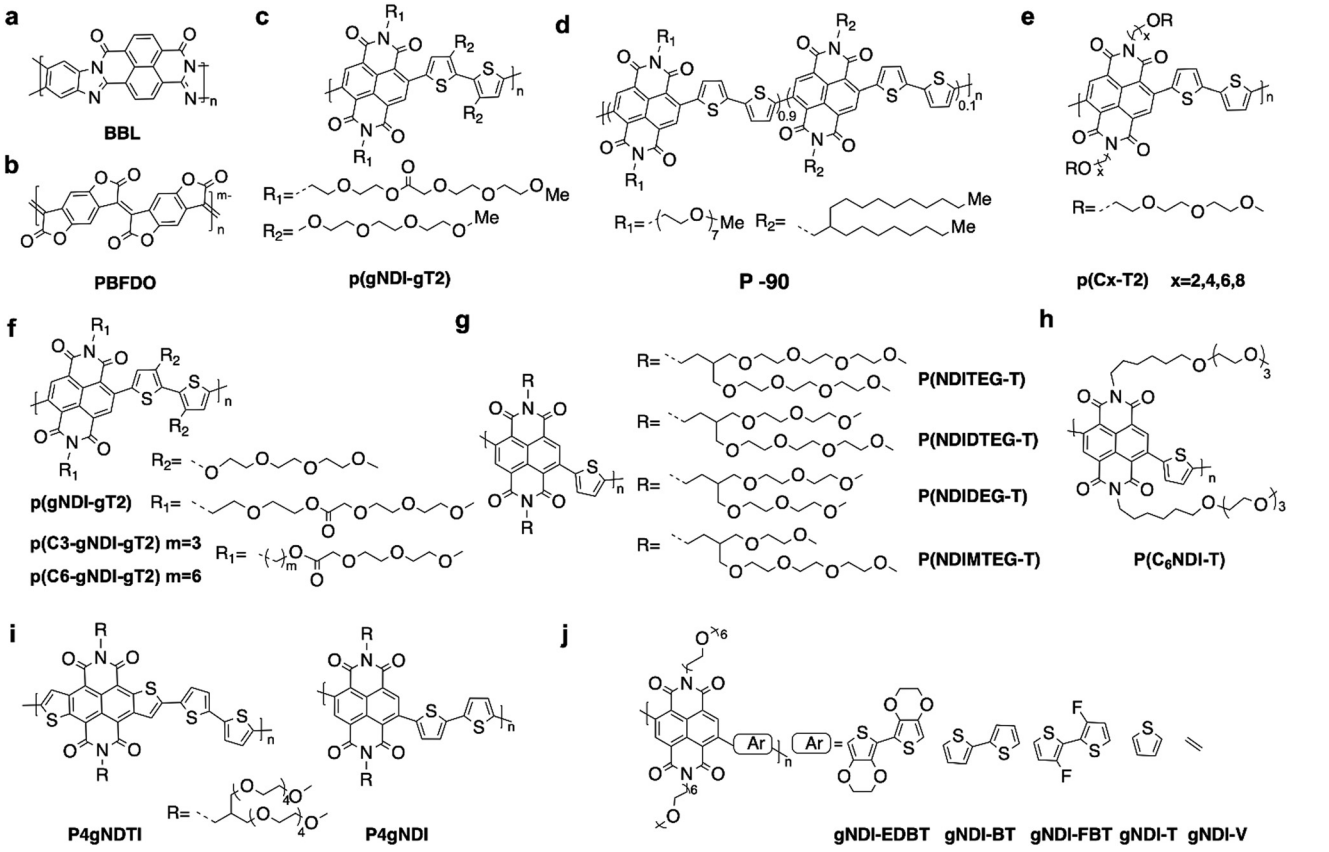

Fig. 3 Chemical structures of n-type (a) and (b) side-chain-free polymers and (c)–(j) NDI derivatives utilized in the OECTs.

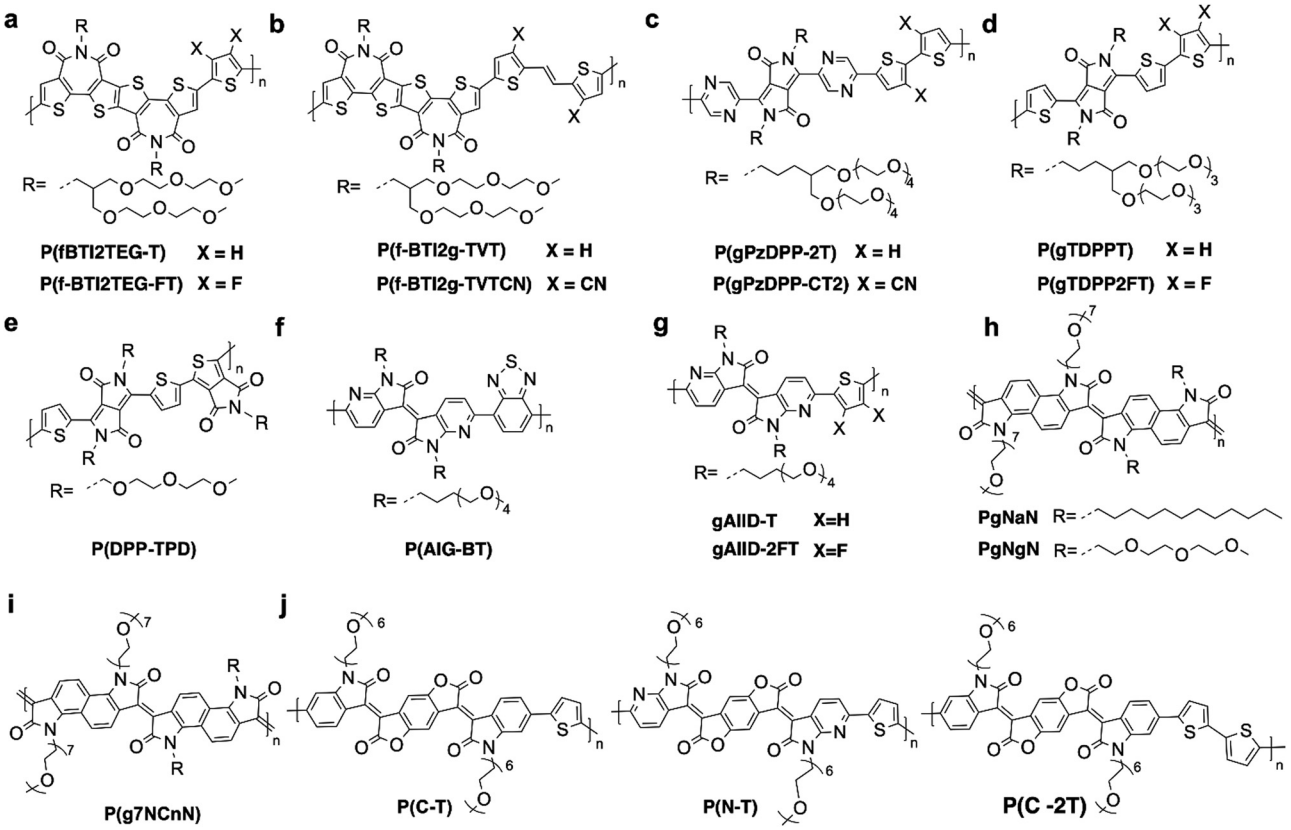

Fig. 4 Chemical structures of the n-type (a) and (b) BTI derivatives, (c)–(e) DPP derivatives, (f) and (g) IID derivatives, (h)–(i) other derivatives and (j) BDOPV derivatives utilized in n-type OECT channel materials.

charge carrier mobility, with values surpassing 10 $cm^2\ V^{-1}\ s^{-1}$ in OFETs[50] which is attributed to their optimal crystallinity that provides many benefits such as high purity, a well-defined structure, ease of synthesis, scalability for industrial use, and consistent structure–property. Additionally, the strategy of adding EG side chains to improve ion penetration while maintaining the π-conjugated backbones for electronic conductivity has been proven to be effective for small molecules used in OECTs.[51]

The charge carrier mobility of n-type OECTs typically ranges from 10^{-4} to 10^{-3} $cm^2\ V^{-1}\ s^{-1}$, while p-type OECTs exhibit higher values ranging from 10^{-1} to 10^{1} $cm^2\ V^{-1}\ s^{-1}$.[14] This significant difference in charge carrier mobility between n-type and p-type OECTs has presented a considerable challenge in the development of n-type OECTs. The lower electron mobilities could be attributed to the electron's susceptibility to water and oxygen.[52] Thus, lowering LUMO energy levels is an effective approach to realizing high-performance n-type OECT materials. Previous research has revealed that the electrochemical window for water and oxygen redox occurs at 3.7 eV and 4.8 eV, respectively, creating potential traps for electrons.[53] Further experimental evidence suggests that energy levels below 4 eV are sufficient for achieving stable electron transport,[1] as the oxygen trapping process requires additional energy to overcome reaction barriers. Encapsulation technology using CYTOP[54,55] has been used in OFETs to prevent water and oxygen exposure. However, this poses a greater challenge for OECTs since they operate in a water environment.

Reducing the LUMO energy level is a common approach in materials design to tackle the instability issue of n-type OECT materials. Donor–acceptor (D–A) or acceptor–acceptor (A–A) type conjugated polymers are widely employed in OECTs, due to their ready structural and energy-level tunability.[56] Several electron-deficient building blocks, such as naphthalene diimide (NDI),[57] diketopyrrolopyrrole (DPP),[58] isoindigo (IID),[59] bithiophene imide dimer (BTI)[60] and benzodifurandione-based oligo(*p*-phenylene vinylene) (BDOPV), have been employed.[61] These building blocks exhibit LUMO levels ranging from −3.4 eV to −4.2 eV,[62] making electron transport more stable. Notably, the LUMO energy level is not the sole determinant for performance in n-type OECTs. Other factors, such as the planarity of the skeleton,[63] electron delocalization,[64] and molecular packing,[65] also play crucial roles in enhancing OECT performance. All reported n-type OECT materials are shown in Fig. 3–5 and their OECT performances are summarized in Tables 1 and 2.

To develop ambipolar OECT-based circuits, ambipolar materials must fulfill stringent requirements, such as high and balanced effective electron and hole mobilities, optimal HOMO and LUMO energy levels for good stability in aqueous environments, and rapid and symmetrical ion transport for both cations and anions.[88] There are two approaches for developing ambipolar materials: (1) synthesizing single-component ambipolar materials and (2) blending p-type and n-type materials in a bulk-heterojunction structure. One effective method to develop single-component

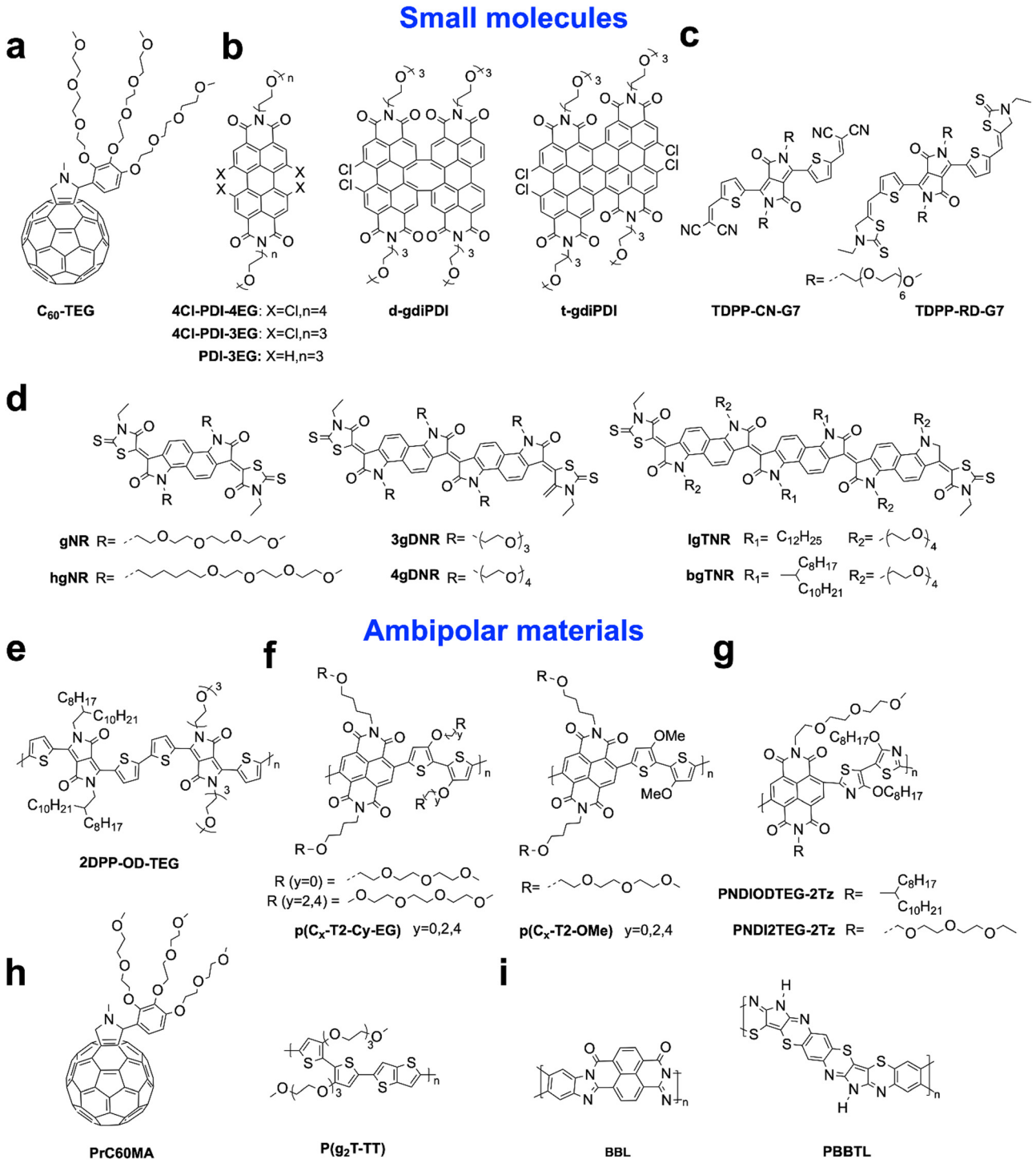

Fig. 5 Chemical structures of (a)–(d) n-type small molecules and (e)–(i) ambipolar materials utilized in OECT channel materials.

ambipolar materials is through the combination of a strong electron acceptor and a strong electron donor, forming D–A polymers with narrow band gaps.[15] The utilization of bulk-heterojunction blends, inspired by organic photovoltaics, is another strategy for developing ambipolar OECT materials. This approach uses the blend of p- and n-type materials in a single layer, enabling the transport of different charge carriers. It offers material selection versatility and does not require synthesizing new materials. Additionally, by adjusting the blend ratios, matched performance can be achieved, providing further advantages.[18,69] All reported ambipolar materials are shown in Fig. 5 and their OECT performance is summarized in Table 3.

3.2 N-Type and ambipolar OECT materials

3.2.1 Side-chain-free polymers. Poly(benzimidazobenzophenanthroline) (BBL, Fig. 3a) was first reported in 1969 and

Table 1 Summary of the OECT performance characteristics of n-type polymers

Materials	μ^a (cm^2 V^{-1} s^{-1})	μC^{*a} (F cm^{-1} V^{-1} s^{-1})	C^* (F cm^{-3})	V_{th} (V)	$g_{m,norm}{}^b$ (S cm^{-1})	τ_{on} (ms)	I_{on}/I_{off}	Cycles and remaining I_D compared to initial I_D	Ref.
BBL	7×10^{-4}	—	—	0.21	0.36	—	900	360, 100%	17
BBL	2.14×10^{-3}	1.99	731	0.19	0.81	5.2	1.6×10^3	—	66
P-90	7.45×10^{-3}	0.0343	261.5	0.24	0.009	41	19.4	—	66
BBL_{15}	$(3.59 \pm 0.23) \times 10^{-3}$	1.94 ± 0.05	540 ± 20	0.27	0.62	0.89	2.9×10^3	1000, 95%	67
BBL_{60}	$(9.42 \pm 0.88) \times 10^{-3}$	4.90 ± 0.16	520 ± 32	0.21	1.92	0.52	8.3×10^4	1000, 95%	67
BBL_{98}	$(2.05 \pm 0.15) \times 10^{-2}$	10.2 ± 0.4	499 ± 19	0.18	4.04	0.43	2×10^5	1000, 95%	67
BBL_{152}	$(4.40 \pm 0.34) \times 10^{-2}$	25.9 ± 0.9	589 ± 26	0.15	11.1	0.38	4.4×10^5	1000, 95%	67
BBL : MWCNT (10 : 1)	1.41×10^{-3}	1.06	753.8	—	0.335	15	—	—	68
PBBTL:BBL	$(0.81 \pm 0.48) \times 10^{-2}$	1.36 ± 0.81	168	0.26	0.43 ± 0.24	1.72	—	—	69
BBL_L	$0.52 \pm 0.08 \times 10^{-3}$	0.28 ± 0.01	539.8 ± 85.8	0.28	0.08	142	1.23×10^4	—	70
BBL_H	$9.2 \pm 1.6 \times 10^{-3}$	9.27 ± 0.03	1007.1 ± 172.8	0.17	3.98	80.3	1.59×10^4	—	70
PBFDO	—	190	—	—	—	—	1.6×10^2	10, 1%	31
p(gNDI-gT2)	1×10^{-5}	—	—	0.28	0.11	5	3.2×10^3	360, ~100%	34
P-50	—	—	—	0.36	0.0067	—	5×10^2	—	49
P-75	1.46×10^{-4}	0.027	188	0.29	0.014	—	5.5×10^2	—	49
P-90	2.38×10^{-4}	0.047	198.2	0.26	0.021	—	4.0×10^3	—	49
P-100	1.96×10^{-4}	0.038	192.4	0.25	0.020	—	1.1×10^3	—	49
P-90	8.0×10^{-5}	0.00624	78	0.25	0.0021	—	10^2	—	71
P90:TBAF (10%)	1.6×10^{-4}	0.02128	133	0.25	0.0075	—	10^2	—	71
P90:TBAF (40%)	1.8×10^{-4}	0.02574	143	0.22	0.0088	—	10^3	1620, ~100%	71
P90:TBAF (80%)	1.6×10^{-4}	0.024	150	0.25	0.0084	—	10^3	—	71
P90	9.8×10^{-6}	0.0009	91.6	0.29	0.00028	—	—	—	72
P90, MBT	1.7×10^{-5}	0.0023	132.5	0.27	0.00076	—	—	—	72
P90, PFBT	1.2×10^{-5}	0.0008	61.9	0.29	0.00027	—	—	—	72
p(NDI-T2-L2)	—	0.31	95	0.22	0.011	40	2.2×10^2	180, ≈	73
p(gNDI-gT2)	2.2×10^{-4}	0.06	221	0.26	0.013	—	—	360, 93%	74
p(C3-gNDI-gT2)	9.2×10^{-4}	0.13	72	0.25	0.034	—	—	900, 119%	74
p(C6-gNDI-gT2)	6.3×10^{-4}	0.16	59	0.37	0.37	—	—	900, 133%	74
p(C_4-T2-C_2-EG)	4.99×10^{-5}	0.01	200	0.30	0.002	6.2	—	—	75
p(C_4-T2-C_4-EG)	5.34×10^{-5}	0.006	116	0.33	0.001	12.5	—	—	75
p(C_2-T2)	3.97×10^{-4}	0.2	492	0.27	0.040	6.3	—	—	75
p(C_4-T2)	1.90×10^{-3}	0.3	158	0.24	0.063	7.5	—	—	75
p(C_6-T2)	4.74×10^{-3}	1.29	272	0.30	0.228	9.6	—	500, 160%	75
p(C_8-T2)	3.76×10^{-4}	0.13	342	0.37	0.015	12.7	—	—	75
P(NDIMTEG-T)	0.24×10^{-3}	0.04	165.8	0.26	0.00075	—	—	100, >100%	76
P(NDIDEG-T)	0.94×10^{-3}	0.21	221.5	0.18	0.0034	—	—	100, >100%	76
P(NDIDTEG-T)	2.12×10^{-3}	0.51	239.9	0.15	0.0090	—	—	100, >100%	76
P(NDITEG-T)	2.23×10^{-3}	0.56	250.9	0.18	0.0095	—	—	100, >100%	76
gNDI-EDBT	3.96×10^{-4}	0.02 ± 0.01	50.5	0.52	0.003	377.6	10^3	360, 100%	77
gNDI-BT	5.69×10^{-4}	0.09 ± 0.01	158.3	0.30	0.019	102.3	10^4	360, 100%	77
gNDI-FBT	6.10×10^{-4}	0.12 ± 0.02	196.6	0.19	0.036	45.5	10^4	360, 100%	77
PNDI2TEG-2Tz	3.16×10^{-3}	1.16 ± 0.28	367	0.54	0.0518	—	10^5	1000, >100%	78
gNDI-V	$1.4 \times 10^{-2} \pm 1.3 \times 10^{-3}$	2.31	144 ± 5	0.30	0.042 ± 0.02	2.90	—	360, 91.2%	63
gNDI-T	$1.5 \times 10^{-3} \pm 2.0 \times 10^{-4}$	0.42	237 ± 8	0.20	0.11 ± 0.01	0.87	—	360, 94.8%	63
P4gNDI	$(7.34 \pm 2.11) \times 10^{-6}$	$(1.61 \pm 0.46) \times 10^{-3}$	219	0.27 ± 0.05	$(1.87 \pm 0.25) \times 10^{-3}$	—	20.2 ± 0.15	180, 94%	79
P4gNDTI	$(1.42 \pm 0.22) \times 10^{-3}$	0.27 ± 0.04	167 ± 11.4	0.20 ± 0.003	0.47 ± 0.06	—	$(4.18 \pm 1.1) \times 10^3$	180, 100%	79
P(fBTI2TEG-T)	0.044	2.30	52	0.68	0.27	322	16.8	300, 70%	60
P(f-BTI2TEG-FT)	0.034	15.20	443	0.54	4.60	272	1.3×10^3	300, 70%	60
P(f-BTI2g-TVT)	0.014	1.50	110 ± 19	0.9	0.27	52	10^2	240, 75%	80
P(f-BTI2g-TVTCN)	0.24	41.3	170 ± 22	0.68	12.8	68	10^5	240, 70%	80
P(gPzDPP-2T)	1.6×10^{-3}	0.22	134	0.56	0.053	22.7	—	100, 50%	64
P(gPzDPPCT2)	1.9×10^{-2}	1.72	91	0.32	0.82	3.0	—	100, 50%	64

Table 1 (*continued*)

Materials	μ^a (cm^2 V^{-1} s^{-1})	μC^{*a} (F cm^{-1} V^{-1} s^{-1})	C^* (F cm^{-3})	V_{th} (V)	$g_{m,norm}$ [b] (S cm^{-1})	τ_{on} (ms)	I_{on}/I_{off}	Cycles and remaining I_D compared to initial I_D	Ref.
P(gTDPP2FT)	0.27 ± 0.04	42.2 ± 6.5	156 ± 24	0.64 ± 0.01	6.75	—	5×10^6	400, 95.2%	14
P(DPP-TDP)	0.11	7.62 ± 0.32	68.58	0.575	1.31	12.5	—	900, 65%	81
P(AIG-BT)	1.4×10^{-3}	0.12 ± 0.03	83.5 ± 8.5	0.55	0.029 ± 0.006	—	—	500, 90%	59
gAIID-T	0.002	0.09 ± 0.01	43.0 ± 3.8	0.59 ± 0.01	0.015	213.3 ± 12	10^4	600, 12.6%	82
gAIID-2FT	0.049	4.09 ± 0.09	99.8 ± 2.0	0.45 ± 0.01	0.94	58.5 ± 6.7	10^5	1200, 100%	82
P(C-T)	0.069	6.7 ± 0.9	97 ± 9	0.43	0.80 ± 0.16	—	—	1000, 18.5%	82
P(N-T)	0.059	4.3 ± 0.6	73 ± 9	0.25	0.72 ± 0.23	—	—	1000, 63%	82
P(C-2T)	0.019	1.0 ± 0.3	53 ± 9	0.44	0.14 ± 0.04	—	—	4200, 72%	82
P(g7NC2N)	(2.00 ± 0.41) × 10^{-3}	0.36 ± 0.074	180 ± 16	0.23 ± 0.0033	0.069 ± 0.012	—	—	180, 75%	83
P(g7NC4N)	(1.46 ± 0.53) × 10^{-3}	0.18 ± 0.067	126 ± 12	0.21 ± 0.0029	0.035 ± 0.013	—	—	180, 100%	83
P(g7NC6N)	(2.29 ± 0.70) × 10^{-3}	0.34 ± 0.111	150 ± 4	0.21 ± 0.0064	0.065 ± 0.019	—	—	180, 100%	83
P(g7NC8N)	(6.01 ± 1.87) × 10^{-3}	1.19 ± 0.371	199 ± 27	0.25 ± 0.0034	0.240 ± 0.076	—	—	180, 100%	83
P(g7NC10N)	(1.20 ± 0.07) × 10^{-2}	1.83 ± 0.101	153 ± 34	0.30 ± 0.003	0.370 ± 0.023	—	—	180, 100%	83
P(g7NC12N)	(6.50 ± 1.01) × 10^{-3}	0.66 ± 0.113	100 ± 6	0.328 ± 0.0053	0.212 ± 0.015	—	—	180, 100%	83
P(g7NC16N)	(3.80 ± 0.59) × 10^{-3}	0.33 ± 0.074	86 ± 11	0.36 ± 0.001	0.047 ± 0.005			180, 50%	83

Means the data are missing in the literature. [a] μC^* and μ are the average data calculated from the g_m when the electrolyte is 0.1 M NaCl aqueous solution. [b] $g_{m,norm}$ values are extracted using the equation $g_{m,norm} = g_m/(W\ d\ L^{-1})$.

initially used as an n-type OECT material by Sun *et al.* in 2018.[12] BBL's high backbone planarity and side-chain-free nature enhanced its interchain interactions, contributing to its exceptional electrochemical stability and a remarkable volumetric capacitance of 930 F cm^{-3} (Table 1). Nonetheless, BBLs' processing is difficult, which requires methanesulfonic acid as the solvent due to its no-side chain.[66] As one of the earliest promising n-type polymers, various approaches have been explored to further enhance BBL's performance in OECTs.[48,67,90] Particularly, increasing the molecular weight of BBL has led to remarkably high values for μC^* (25.9 F cm^{-1} V^{-1} s^{-1}) due to enhanced stronger π–π interaction and higher crystallinity.[79] This establishes a solid basis for the practical application of stable and high-performance n-type OECT materials. Very recently, Ginger *et al.* discovered that BBL films undergo irreversible hydration during the initial electrochemical doping cycle, resulting in significant water retention and expansion of the lamellar structure. Surprisingly, this hydration process creates a hydrophilic environment that facilitates rapid ion hydration, without affecting the crystallization of BBL despite its rigid backbone and the absence of hydrophilic side chains.[70] The findings suggest the promising potential of side chain-free polymers in OECTs.

In 2022, a breakthrough in performance was made by Huang *et al.* in no-side-chain polymers. They reported a highly conductive n-type polymer called PBFDO (Fig. 3b), with exceptional performance (180 F cm^{-1} V^{-1} s^{-1}, Table 1) due to its tightly micro-stacking structure and high backbone planarity.[31] However, this study lacks detailed data about OECT parameters, hindering further analysis. To evaluate its potential in OECT sensing applications, we conducted performance tests by using commercially available material PBFDO. While its transconductance is high, the stability of PBFDO is poor, leading to significant degradation after just a few on–off cycles. Moreover, the on/off ratio of PBFDO is also small ($\sim 10^2$), which is four orders of magnitude smaller than that of reported high-performance n-type OECT material P(gTDPP2FT) ($I_{on/off} \sim 6 \times 10^5$).[14] Thus, it cannot be considered as a promising material for practical applications.

3.2.2 NDI derivatives. Naphthalene diimide (NDI) is a popular building block in OECTs. In 2016, McCulloch *et al.* reported the first ambipolar OECT material named p(gNDI-gT2) (Fig. 3c) with stable n-type charge transport behaviors. However, the low electron mobility restricts its ability to generate high currents and transconductances.[34] Subsequently, they conducted a systematic investigation to assess the impact of polar glycol chains on the performance of OECTs by varying the ratios of glycol to alkyl side chains in NDI-T2 copolymers. As the percentage of glycol chains increased to 50%, the polymer began to exhibit OECT performance, and the best results were achieved with P-90 (containing 90% of glycol side chains, Fig. 3d), showcasing an electron mobility of 2.38 × 10^{-4} cm^2 V^{-1} s^{-1} (Table 1). Thus, the addition of alkyl side chains has a significant influence on the swelling in aqueous electrolytes.[49] Notably, NDI-T2 copolymers with alkyl chains show higher electron mobilities, while the electron mobility drops by more than 2 orders of magnitude when more than 25% of the alkyl chains are replaced by polar glycol

Table 2 Summary of OECT performance characteristics of n-type small molecules

Materials	μ^a ($cm^2\ V^{-1}\ s^{-1}$)	μC^{*a} ($F\ cm^{-1}\ V^{-1}\ s^{-1}$)	C^* ($F\ cm^{-3}$)	V_{th} (V)	$g_{m,norm}{}^b$ ($S\ cm^{-1}$)	τ_{on} (ms)	I_{on}/I_{off}	Cycles and remaining I_D compared to initial I_D	Ref.
C60-TEG	0.03	7.0 ± 2.0	20 ± 50	0.55	0.35	80	2.5×10^4	50, 60%	84
gNR	0.013	2.5 ± 0.1	198	0.35 ± 0.01	0.402 ± 0.01	—	6×10^4	360, 11.3%	43
hgNR	0.009	1.2 ± 0.04	129	0.29 ± 0.01	0.263 ± 0.003	—	4×10^4	360, 56.3%	43
gNR-CF	1.25×10^{-2}	2.48 ± 0.11	198 ± 12	0.36 ± 0.01	0.384	158	—	600, 7.3%	85
gNR-3FOH	1.40×10^{-2}	3.78 ± 0.13	272 ± 11	0.26 ± 0.01	1.119	117	—	600, 63.9%	85
gNR-6FOH	1.78×10^{-2}	5.12 ± 0.13	288 ± 12	0.32 ± 0.01	1.216	94	—	600, 61.6%	85
gNR-9FOH	1.13×10^{-2}	3.80 ± 0.18	336 ± 16	0.34 ± 0.01	0.875	214	—	600, 75.2%	85
3gDNR	4.3×10^{-2}	9.4 ± 0.9	217 ± 23	0.27 ± 0.01	2.16 ± 0.20	439 ± 22	$\sim 10^4$	300, 57.5%	86
4gDNR	2.1×10^{-2}	4.7 ± 0.5	225 ± 26	0.25 ± 0.01	1.17 ± 0.13	207 ± 18	$\sim 10^4$	300, 53.9%	86
IgTNR	0.03	3.9 ± 0.3	141 ± 10	0.35 ± 0.01	0.97 ± 0.05	308 ± 19	—	300, 37%	87
bgTNR	0.29	28.4 ± 3.2	106 ± 8	0.29 ± 0.01	7.1 ± 0.5	489 ± 24	—	300, 37%	87
4Cl-PDI-4EG	$(4.18 \pm 0.18) \times 10^{-4}$	0.13 ± 0.05	303 ± 17	0.05	0.0452	215	$\sim 10^4$	600, 94%	83
4Cl-PDI-3EG	$(8.07 \pm 0.71) \times 10^{-4}$	0.17 ± 0.03	198 ± 25	0.26	0.0484	282	$\sim 10^4$	600, 87%	83
PDI-3EG	$(3.79 \pm 0.10) \times 10^{-4}$	0.08 ± 0.02	207 ± 8	0.34	0.0164	130	$\sim 10^3$	600, 88%	83
t-gdiPDI	8.3×10^{-4}	0.21 ± 0.02	254 ± 7	−0.07 ± 0.01	0.055 ± 0.004	123 ± 6	$\sim 10^3$	1200, >100%	32
d-gdiPDI	5.3×10^{-4}	0.34 ± 0.01	628 ± 29	0.11 ± 0.01	0.17 ± 0.046	87 ± 9	$\sim 10^3$	1200, >100%	32
TDPP-CN-G7	5×10^{-3}	0.68 ± 0.11	165.2 ± 16.1	0.16	0.23	—	$\sim 10^4$	40, 20%	33
TDPP-RD-G7	7.5×10^{-2}	5.43 ± 0.37	78.6 ± 7.5	0.34	2.2	10.5	$\sim 10^4$	100, 70%	33

Means the data are missing in the literature. [a] μC^* and μ are the average data calculated from the g_m when the electrolyte is 0.1 M NaCl aqueous solution. [b] $g_{m,norm}$ values are extracted according to the equation $g_{m,norm} = g_m/(W\ d\ L^{-1})$.

Table 3 Summary of the OECT performance characteristics of ambipolar materials

Materials	Transporting type	μC^{*a} ($F\ cm^{-1}\ V^{-1}\ s^{-1}$)	μ^a ($cm^2\ V^{-1}\ s^{-1}$)	V_{th} (V)	$g_{m,norm}{}^b$ ($S\ cm^{-1}$)	Cycles and remaining I_D compared to initial I_D	Ref.
p(gNDI-gT2)	n	0.18	—	0.35	0.109	360, 100%	34
	p	—	—	—	0.067	—	
2DPP-OD-TEG	n	6.8	—	0.89	1.28	80, 100%	15
	p	31.8	—	−0.82	3.87	80, 10%	
p(C_4-T2-C_0-EG)	n	0.22 ± 0.016	1.16×10^{-3}	0.32 ± 0.007	0.31	—	75
	p	—	—	—	—	—	
p(C_4-T2-OMe)	n	0.07 ± 0.011	3.87×10^{-4}	0.46 ± 0.03	0.10	—	75
	p	—	—	—	—	—	
PNDIODTEG-2Tz	n	2.34	—	0.75	0.117	—	89
	p	—	—	—	—	—	
PNDI2TEG-2Tz	n	1.16	—	0.54	0.493	—	89
	p	—	—	—	—	—	
PrC60MA : p(g2T-TT) 95 : 5 (w:w)	n	11.8 ± 1.4	—	0.649	3.0 ± 0.6	100, 100%	18
	p	22.8 ± 0.9	—	−0.09	4.8 ± 0.2	100, 100%	
BBL : PBBTL = 1 : 3	n	1.36 ± 0.81	0.008 ± 0.005	—	0.43 ± 0.24	5000, 100%	69
	p	2.72 ± 1.04	0.022 ± 0.008	—	0.41 ± 0.17	5000, 90%	

Means the data are missing in the literature. [a] μC^* values are the average data calculated when the electrolyte is 0.1 M NaCl aqueous solution. [b] $g_{m,norm}$ values are extracted according to the equation $g_{m,norm} = g_m/(W\ d\ L^{-1})$.

chains. This decline in mobility is attributed to the polymer's swelling in water and its interaction with cations when utilized in OECTs.

In a subsequent study, Inal *et al.* examined the impact of alkyl spacers in the polar glycol chains on the NDI-T2 backbone (p(C*x*-T2), Fig. 3e). They found that while a two-carbon spacer achieved maximum water uptake, the addition of a six-carbon spacer resulted in a ten-fold improvement, primarily due to a significant increase in electron mobility (μ of 4.74×10^{-3} $cm^2\ V^{-1}\ s^{-1}$, Table 1). Further analysis using GIWAXS revealed that the presence of more oriented and robust crystallites contributed to the higher electron mobility. Additionally, a similar result has been observed by Kim and Yoon *et al.*; they found that the shortest asymmetrical side chains[76] (P(NDIMTEG-T), Fig. 3g) exhibited the best doping properties and improved performance, probably due to the enhanced edge-on oriented backbone crystallinity. Notably, when an ethanol/water-based solution process was used to fabricate OECTs instead of chloroform, the μ value of P(NDIMTEG-T) tripled to 2.23×10^{-3} $cm^2\ V^{-1}\ s^{-1}$, attributed to strengthened edge-on oriented crystalline structures. These studies demonstrate the importance of molecular packing in achieving high electron mobility, which can be achieved not only by tuning the side chains but also by optimizing processing conditions.

In 2020, Inal *et al.* investigated why the side-chain free polymer BBL performs significantly better in OECTs than the

NDI derivatives, P90.[66] BBL shows longer coherence lengths, shorter π-stacking distances and maintains good molecular packing during doping, leading to enhanced stability. The planarity of the BBL backbone and the absence of ion-coordinating side chains were identified as key factors contributing to its superior performance. These findings emphasize the significance of backbone engineering strategies. For instance, McCulloch *et al.* replaced the electron-deficient NDI unit with the extended naphthodithiophene diimide (NDTI) unit, resulting in a more rigid structure and reduced rotational torsion. This led to a planar backbone and tighter packing in P4gNDTI (Fig. 3i), resulting in a remarkable improvement in electron mobility and μC^* by over two orders of magnitude, along with increased stability.[79] Similarly, Yue *et al.* explored variable donating companion moieties in combination with glycolated NDI, and their use of vinylene (gNDI-V, Fig. 3j) promoted a coplanar backbone conformation and improved thin-film crystallinity through hydrogen bonding.[63] Remarkably, gNDI-V exhibited high electron mobility (0.014 $cm^2 V^{-1} s^{-1}$) and μC^* (2.31 F $cm^{-1} V^{-1} s^{-1}$) (Table 1) in NDI-based copolymers. These results demonstrate that enhancing backbone planarity is an effective approach to achieving high-performance materials.

3.2.3 BTI derivatives. The bithiophene imide dimer (BTI) is a novel imide functionalized heteroarene, possessing good solubility, a flat backbone, and exhibits minimal interference with neighboring heteroarenes.[68] Various strategies, including ring fusion, thiazole substitution, fluorination, cyanation, and chalcogen substitution, have been proven effective to increase its electron affinity,[91] making it one of the promising polymers for designing n-type polymers. Guo *et al.* reported two types of polymers by using fused BTI2 (f-BTI2) as the acceptor, due to its deep LUMO energy and high backbone planarity. They mainly studied the effectiveness of introducing fluorine atoms or cyano groups into the donor. In 2021, they reported two D–A type polymers (namely f-BTI2TEG-T and f-BTI2TEG-FT, Fig. 4a), consisting of f-BTI2 and thiophene/difluorothiophene as the donor. Branched OEG side chains were introduced on f-BTI2 to ensure sufficient polymer solubility. Both polymers show a high backbone planarity with dihedral angles smaller than 1 degree between f-BTI2 and the donor. Additionally, the introduction of fluorine atoms effectively decreases the polymers' crystallinity, which promotes ionic conduction. As a result, f-BTI2TEG-FT demonstrates significantly improved C^*, while f-BTI2TEG-T shows similar electron mobility in OECTs. Consequently, f-BTI2TEG-FT-based[60] OECTs achieved a maximum μC^* of 15.2 F $cm^{-1} V^{-1} s^{-1}$ (Table 1).

Driven by the great success of f-BTI2 with reduced steric hindrance, in the following study, they introduced thienylene–vinylene–thienylene (TVT)/cyano-functionalized TVT as the donor to enlarge the backbone length. Firstly, the remarkable planarity of both polymers, with a minimal torsion angle ($<0.1^\circ$), suggests that the incorporation of the cyano group into the TVT unit does not compromise the planarity of the f-BTI2g-TVTCN backbone. Additionally, compared to the non-cyanoed f-BTI2g-TVT, f-BTI2g-TVTCN shows a lower LUMO energy level of –3.81 eV, improving its ability to inject electrons. Furthermore, the introduction of cyano reduces its donor–acceptor character, enhancing polaron delocalization. When used as the channel in OECT, f-BTI2g-TVTCN (Fig. 4b) exhibited an outstanding μ of 0.24 $cm^2 V^{-1} s^{-1}$ and μC^* of 41.3 F $cm^{-1} V^{-1} s^{-1}$ (Table 1).[80]

3.2.4 DPP derivatives. Diketopyrrolopyrrole (DPP), containing a central pyrrole ring with two adjacent carbonyl groups, is a strong electron-deficient building block. It has high planarity with strong π–π interactions, leading to efficient interchain charge transport.[92] DPP derivatives have undergone extensive exploration and utilization in the development of high-mobility conjugated polymers.[62] DPP derivatives have been successfully used in a variety of high-performance p-type OECT materials,[78] In 2022, Lei *et al.* developed the first DPP-based n-type OECT materials by copolymerizing pyrazine-flanked DPP (PzDPP) and bithiophene units. PzDPP has the lowest LUMO in all the DPP derivatives and was chosen to lower the LUMO energy level. Additionally, the structural design enables noncovalent interactions between the pyrazine protons and carbonyl oxygen atoms as well as the thiophene protons, contributing to the polymer's remarkably flat backbone. When introducing the cyano group into the bithiophene unit, it lowers the LUMO energy level down to −4.19 eV. Furthermore, the cyanide P(gPzDPP-CT2) (Fig. 4c) improved the polymers' planarity and rigidity, particularly when in the reduced state and achieved a uniform distribution of negative polarons along the polymer backbone.[64] Consequently, P(gPzDPP-CT2) exhibited an increased electron mobility of 1.6×10^{-2} $cm^2 V^{-1} s^{-1}$ and μC^* of 1.72 F $cm^{-1} V^{-1} s^{-1}$. However, this polymer is not stable under cycling (50% drop in current after 100 cycles, Table 1), despite having a very low LUMO level.

Afterward, Lei *et al.* found that the LUMO energy levels of polymers do not correlate with their n-type performance in OECTs. They synthesized two polymers, P(gTDPPT) and P(gTDPP2FT) (Fig. 4d), to explore the design strategies for high-performance n-type OECT materials. Compared with P(gTDPPT), which shows typical p-type behaviors, fluorine substitution on the thiophene unit yielded an n-type OECT material with high electron mobility of 0.35 $cm^2 V^{-1} s^{-1}$, high μC^* of 54.8 F $cm^{-1} V^{-1} s^{-1}$ (Table 1), and fast response speed of τ_{on}/τ_{off} = 1.75/0.15 ms.[14] Notably, P(gTDPP2FT)'s LUMO energy level (−3.86 eV) is higher than that of P(gPzDPP-CT2) (−4.19 eV), indicating that a low-lying LUMO energy level does not necessarily correlate with high n-type performance. Their experimental and theoretical analyses revealed that the doped state stability, backbone planarity, and charge distribution contributed to the superior performance of P(gTDPP2FT), which is concluded as ''doped state engineering''. Because OECT materials usually work under highly doped states, their stability, backbone structure, and electronic structures are largely different from conventional OFET materials, which mainly work under a lightly doped state. Thus, ''doped state engineering'' provides a new design direction for high-performance n-type OECT polymers.

Very recently, aiming at designing polymers with maximum electron affinity and a highly planarized backbone, Thelakkat *et al.* synthesized an A–A type polymer, P(DPP-TPD) (Fig. 4e) by combining thiophene DPP (TDPP) with thienopyrrolodione (TPD). The A–A type design with only electron-deficient acceptors

can effectively lower the LUMO energy level. Moreover, TDPP and TPD were chosen to mimic the ladder-type polymers, between the thiophene protons and carbonyl oxygen atoms. Furthermore, both monomers are equipped with triethylene glycol substituents, where noncovalent interactions are formed to ensure ion compatibility as well as sufficient solubility. As a result, P(DPP-TPD) exhibited a deep LUMO energy level at −4.15 eV and an average μC^* of 7.62 F cm^{-1} V^{-1} s^{-1} (Table 1) in OECT.[81] This result further proves the previous conclusion that the LUMO energy level of the polymers is not well correlated to its n-type performance in OECT.

3.2.5 IID and BDOPV derivatives. Isoindigo (IID) is another promising electron-deficient building block, with a readily functionalized and highly planar backbone.[93] In 2022, B. Nielsen *et al.* reported a series of IID polymers based on different building blocks, including electron-deficient 2,1,3-benzothiadiazole (BT) and electron-rich thiophene derivatives (T).[63] Among them, only AIG-BT (Fig. 4f) showed n-type performance with an electron mobility of 1.4 × 10^{-3} cm^2 V^{-1} s^{-1} (Table 1). Calculations and experiments demonstrated that the formation of n-type OECT materials can be attributed to several factors, including relatively high electron affinity, efficient electron delocalization, and highly coplanar geometry with consistent conformational uniformity which facilitates strong π–π stacking interactions. Additionally, TIG-T exhibited good p-type performance with a μC^* of 132 F cm^{-1} V^{-1} s^{-1}. It proves the potential of IID derivatives in designing both n-type and p-type OECT materials. However, the n-type performance still lags far behind the p-type ones. Very recently, Yue *et al.* proved that the introduction of fluorine atoms on the donor moieties in IID polymers can effectively improve both the performance and stability of the materials in OECTs. They reported two n-type conjugated polymers based on glycolated 7,7′-diazaisoindigo (AIID) and thiophene units (Fig. 4g).[82] The fluorinated polymer gAIID-2FT showed a deep LUMO level, tightly packed films, and stable film morphology. As a result, it displayed better performance with a μC^* of 4.09 F cm^{-1} V^{-1} s^{-1} and transconductance that maintained 98% of its initial values after 28 days.

Based on IID, a novel structure benzodifurandione-based oligo(*p*-phenylene vinylene) (BDOPV) was developed by breaking the double bond between two lactam rings and inserting a π-conjugated lactone.[93] It is regarded as one of the most electron-deficient building blocks reported to date, with a LUMO energy level of −4.24 eV. Moreover, BDOPV has four carbonyl groups forming four intramolecular hydrogen bonds with the neighboring phenyl protons, leading to a locked and highly planar backbone plane. In 2022, Yue *et al.* found that reducing the LUMO energy level can effectively lower the threshold voltage in OECTs. They reported a series of n-type BDOPV-based polymers by polymerizing the BDOPV with thiophene units.[82] Polymer P(C-T) (Fig. 4j) exhibited a deep-lying LUMO of −4.25 eV. Building upon P(C-T), P(N-T) (Fig. 4j) converts phenyl to pyridine in bisisatin, further reducing the LUMO level to −4.48 eV. When used in OECTs, p(N-T) with a deeper LUMO level, exhibited a low threshold voltage of 0.25 V, compared to that of p(C-T) (0.43 V); however, p(C-T) showed a slightly better μC^*. They proposed that the low-lying LUMO energy levels decrease the energetic barrier of ion injection into the conjugated polymers. Additionally, they designed P(C-2T) (Fig. 4j) by replacing the thiophene with a bithiophene unit, which has a LUMO level of −4.19 eV and higher threshold voltage at 0.44 V in OECTs, consistent with the observed trend. However, P(C-2T) exhibited poor OECT performance. AFM and GIWAXS data revealed that compared to p(C-2T), p(C-T) and P(N-T) exhibited a porous and disordered amorphous microstructure, which could facilitate efficient ion-to-electron coupling and lead to excellent device performance.

3.2.6 Other building blocks. In 2020, McCulloch *et al.* introduced an A–A type fused polymer for n-type OECTs. To avoid the detrimental effects of twisting between single bonds, which can lead to conformational disorder and negatively affect the carrier mobility of the polymer, they developed polymers PgNgN and PgNaN[59] (Fig. 4h), with deep LUMO energy levels below −4.0 eV. However, the rigid backbone structure of PgNgN has poor solubility, resulting in a low molecular weight after polymerization. When introducing 50% alkyl side chains, PgNaN showed improved solubility with a higher molecular weight. PgNaN demonstrates high OECT performance with μC^* of 0.662 F cm^{-1} V^{-1} s^{-1} (Table 1). Afterward, they systemically investigated the ratio of alkyl to glycol side chains with the same backbone (namely p(g$_7$NC$_n$N), Fig. 4i),[83] and concluded that adjusting side chains can effectively improve the OECT performance by enhancing the polymers' molecular weights. As the alkyl side chain length increases from (C2) to (C16), the polymer's number-average molecular weight (M_n) gradually rises from 6.2 kDa to 24.2 kDa. This increase in length leads to higher electron mobility, reaching a peak value of 1.20 × 10^{-2} cm^2 V^{-1} s^{-1} for p(g$_7$NC$_{10}$N). However, the electron mobility decreases by nearly 70% when going from (C10) to (C16) due to the preferential mixed edge-on and face-on stacking of the C10 alkyl chain. Additionally, the p(g$_7$NC$_n$N) polymers were also demonstrated to show high performance in organic thermoelectrics (OTEs), suggesting that OECT and OTE materials might share similar molecular design rules as they are both heavily doped systems.

3.2.7 n-Type small molecules. The first n-type small molecule used in OECTs is C60-TEG (Fig. 5a), a fullerene derivative with glycolate side chains, which was reported by Ginger *et al.*[84] It showed an impressive μC^* value of 7 F cm^{-1} V^{-1} s^{-1} (Table 2). Despite this achievement, the limited structural tunability, high cost, and thermal/photochemical instability of fullerene derivatives have hindered further progress. Yue *et al.* have made significant advancements in the field of non-fullerene n-type small-molecule semiconductors based on the PDI and fused lactam ring derivatives. In 2022, they introduced glycolated perylene diimides (PDI)-derivatives for n-type small-molecule OECT materials.[83] The LUMO energy level was effectively reduced by chlorination of the PDI bay area. Moreover, they observed that the EG side-chain length made a trade-off between electron mobility and film capacitance. As a result, 4Cl-PDI-3EG (Fig. 5b) achieved a maximum μC^* value of 0.2 F cm^{-1} V^{-1} s^{-1}.

Afterward, they further extended the π-conjugation by homo-coupling the PDI derivatives reported above, utilizing two different types of linkages: doubly and triply linked (d-gdiPDI

and t-gdiPDI, Fig. 5b).[32] They aimed to investigate the changes in backbone conformation on OECT performance. DFT calculations revealed that d-gdiPDI exhibits a highly twisted structure, whereas t-gdiPDI possesses a rigid and nearly planar backbone. The highly twisting backbone exerts a favorable influence on the charge storage property. When combined with an ionic gel, d-gdiPDI demonstrated a high specific capacitance of 479 F g^{-1} at a current density of 1 A g^{-1}. Furthermore, d-gdiPDI realizes a remarkably high volumetric capacitance of 657 F cm^{-3}, much higher than that of t-gdiPDI (261 F cm^{-3}). However, the restricted electron mobility of d-gdiPDI hampers its OECT performance.

Furthermore, they developed a novel class of small-molecule OECT materials based on the fused lactam rings. This achievement was realized through the combination of electron-deficient naphthalene bis-isatin (NB) and rhodanine (RD) units. NB, comprising two electron-deficient symmetrical lactam rings with aromatic naphthalene, has been considered a robust building block for constructing ladder-type polymers.[94] RD is also a strong electron-withdrawing unit due to its ketone and thioketone groups on the five-membered aza ring. The resulting material gNR (Fig. 5d) comprises the rigid skeleton and EG side chains, showing a low-lying LUMO level of around −4.0 eV.[43] Furthermore, a highly planar configuration has been achieved in gNR with a near-zero (*ca.* 0.01 Å) dihedral angle between NB and RD, attributed to the non-covalent S–O interactions and hydrogen bonds formed. gNR exhibited good n-type OECT performance with a μC^* of 2.6 F cm^{-1} V^{-1} s^{-1} (Table 2).

In subsequent studies, Yue *et al.* found that extending the π-conjugation in fully fused skeletons is an effective way to optimize the performance of n-type small-molecule OECT materials. By extending the core with a second naphthalene bis-isatin moiety while maintaining the rhodanine end groups, they yielded 3gDNR (Fig. 5d). This extension led to the 3gDNR having a similarly deep LUMO energy level and a highly planar configuration. Furthermore, GIWAXS demonstrated that 3gDNR exhibited predominantly edge-on orientations and a closer π–π stacking distance compared to gNR, which displayed mixed orientations. Ultimately, 3gDNR-based OECT devices achieved a much-improved μC^* of 10.3 F cm^{-1} V^{-1} s^{-1}.[86] Afterwards, they continued extending the conjugation length with three naphthalene bis-isatin moieties, resulting in bgTNR (Fig. 5d). Remarkably, the performance of bgTNR further increased with a high μC^* value of 32.4 F cm^{-1} V^{-1} s^{-1} (Table 2).[87] These improvements were attributed to changes in molecular packing and the formation of tighter π–π stacking. However, the poor operational stability and the complicated synthetic steps of these lactam derivative-based small molecules limited their practical applications.

Recently, Lei *et al.* reported two small molecules with the TDPP as the building block and two electron-deficient malononitrile (CN) and RD as the end functional groups.[33] TDPP-RD-G7 (Fig. 5c) was capable of forming J-type supramolecular polymers and ''polymer-like'' networks, which can enhance its charge transport and reduce its susceptibility to ion diffusion. It achieved a high μC^* of 5.43 F cm^{-1} V^{-1} s^{-1} (Table 2). Their results suggest that the design of molecules with strong intermolecular interactions capable of forming ''polymer-like'' networks is an effective strategy for developing high-performance small-molecule OECT materials.

3.2.8 Ambipolar materials. The first reported ambipolar OECT material is p(gNDI-gT2) (Fig. 3c), in which both NDI and T2 monomers were substituted with linear EG side chains. It exhibited n-type performance of 0.18 F cm^{-1} V^{-1} s^{-1} (Table 3) and long-term stability with no current decrease after 2 h cycling operation. In addition, it also exhibits relatively weak p-type properties. Afterward, Inal *et al.* found when the T2 unit in NDI-T2 was substituted with OMe or EG groups (*e.g.* p(C_4-T2-C_0-OMe) and p(C_4-T2-C_0-EG), Fig. 5f),[75] the increase in HOMO levels led to the shrinkage of the energy gap, resulting in ambipolar materials, but at the expense of n-type performance. When comparing the properties of p(C_4-T2-C_0-OMe) and the n-type polymer p(C_4-T2) with no substituents on the T2 unit, p(C_4-T2-C_0-OMe) exhibits p-type character but the n-type performance (μC^*) drop significantly from 0.30 F cm^{-1} V^{-1} s^{-1} in p(C_4-T2) to 0.07 F cm^{-1} V^{-1} s^{-1}. In the following, when changing the substituent on the T2 unit from OMe to EG in p(C_4-T2-C_0-EG), there was a slight recovery in n-type transport characteristics but a decrease in p-type performance. As a result, p(C_4-T2-C_0-OMe) shows relatively matched ambipolar properties with the n-type of 0.16 F cm^{-1} V^{-1} s^{-1} and p-type of 0.13 F cm^{-1} V^{-1} s^{-1}. However, the performance of ambipolar materials still lags significantly behind.

In 2022, van de Burgt *et al.* reported two ambipolar materials by copolymerizing NDI and dialkoxybithiazole (2Tz). 2Tz has been used to improve the planarity and rigidity of the backbone. The density of TEG side chains has been investigated in this study. PNDI2TEG-2Tz (2TEG) (Fig. 5g), with higher TEG side chains, realized an n-type performance with μC^* of 1.16 F cm^{-1} V^{-1} s^{-1} and μ of 3.16×10^{-3} (Table 3) in OECTs, significantly better than its p-type performance. When half of the triethylene glycol (TEG) side chains are replaced by alkyl side chains, the resulting polymer PNDI2OEG-2Tz (Fig. 5g) exhibited performance degradation in both p-type and n-type due to the increase of π–π stacking and negative change in orientation.

Except for the NDI polymers, DPP polymers also have the potential to develop high-performance ambipolar materials for OECTs. In 2021, B. Aetukuri *et al.* introduced a DPP-based polymer 2DPP-OD-TEG by using two TDPP units and functionalized with 2-octyl dodecyl (OD) and TEG side chains (Fig. 5e).[15] This polymer demonstrated appropriate LUMO energy levels that align well with the electrochemical window of water, ensuring stable n-type OECT operation in the aqueous environment. Notably, 2DPP-OD-TEG displayed good ambipolarity with enhanced performance and a balanced threshold voltage, achieving a μC^* of 6.8 F cm^{-1} V^{-1} s^{-1} for n-type operation and 31.8 F cm^{-1} V^{-1} s^{-1} (Table 3) for p-type operation. However, the stability of its p-type performance is poor (current dropped by 90% under 100 cycles), limiting its application.

The utilization of bulk-heterojunction blends is another notable strategy for developing ambipolar OECT materials. One example involves blending the p-type polymer p(g_2T-TT)

with the n-type fullerene derivative PrC60MA (Fig. 5h).[18] The p(g_2T-TT) polymer is a well-studied and high-performance p-type OECT material and PrC60MA shares a similar fullerene structure to C60-TEG. Through precise optimization of the blend ratio between p(g_2T-TT) and PrC60MA at a weight ratio of 95 : 5, comparable figures of merit (μC^*) were attained for both n-type and p-type operation in OECTs. The n-type performance reached 11.8 F cm^{-1} V^{-1} s^{-1}, while the p-type performance achieved 22.8 F cm^{-1} V^{-1} s^{-1} (Table 3). Moreover, the resulting blend exhibits good stability for both polar, with minimal current degradation after 100 cycles of alternating polarities, thanks to its well-developed interpenetrating network. Another approach involves blending two ladder-type polymers, BBL and PBBTL (Fig. 5i).[69] PBBTL was chosen due to its similar no-side-chain structure to the state-of-the-art BBL, allowing the blends to be processed using acid-based solvents simultaneously. This blending technique enables precise control over mixing and phase separation, leading to the formation of a bicontinuous network with balanced ambipolar properties. The optimal blend ratio is PBBTL : BBL = 3 : 1, which exhibits a μC^* of 2.72 F cm^{-1} V^{-1} s^{-1} for n-type and a μC^* of 1.36 F cm^{-1} V^{-1} s^{-1} for p-type. Additionally, the p- and n-channel components of the blend demonstrate excellent stability, maintaining approximately 90% and 100% of the initial current, respectively, after 5000 pulsed measurement cycles.

To date, single-component ambipolar materials with high and balanced ambipolar properties remain limited. Although the blending technique has emerged as a promising approach, it still faces challenges including low performance, imbalanced hole and electron transport properties, and potential phase stability and reproducibility issues. Given that this field is still in its nascent stages, we expect more systematic studies to drive further advancement.

3.3 Stability of n-type and ambipolar OECT materials

The stability of OECT refers to the ability to maintain its performance during and after continuous operation, which is an essential aspect of practical applications. One common way to evaluate the operational stability of OECT materials is by monitoring the change in drain current during cycling tests. Long-term operational stability in OECTs has been a long-standing challenge due to the electrochemical doping mechanism involved, which is influenced by various factors. Operational stability in OECTs has been widely investigated for p-type materials and devices.[95] With the development of n-type materials in recent years, although the performance has been gradually improved, most of the reported high-performance n-type materials have limited stability. In addition, single-component ambipolar OECT materials with both high p-type and n-type stability have not been reported yet.[15] Therefore, it is very important to improve the stability of n-type and ambipolar materials. Note that due to their sensitivity to water and oxygen, the operational stability of n-type OECT materials brings greater challenges than p-type materials.

First, introducing the alkyl side chains has been proven to effectively improve the operational stability of n-type materials. In 2021, Nelson *et al.* reported that the addition of hydrophobic alkyl side chains to NDI-T2 polymers improves their electrochemical stability by reducing water absorption.[41] The reversible formation of the dipole state is achieved when limited water is absorbed, but uncontrolled expansion may disrupt polymer chain interactions, hindering the transition between single- and double-charged states and causing irreversible changes (Fig. 6a). The negative impact of excessive water absorption on operational stability is further demonstrated experimentally. Maria and Giovannitti *et al.* conducted a study to enhance the electrochemical stability of p(gNDI-gT2) by introducing alkyl spacers between the NDI units and the EG units.[74] p(C3-gNDI-gT2) (Fig. 3f), featuring propyl (C3) spacers, exhibited an approximately 19% increase in operational stability after 900 cycles, while p(C6-gNDI-gT2) with hexyl (C6) spacers showed no change in stability under the same operating conditions. In contrast, p(gNDI-gT2) retained only 67% of its initial performance after 900 cycles. A quartz crystal microbalance with dissipation monitoring has been used to investigate the swelling property. The results revealed that the passive and active swelling of the polymers gradually decreased with increasing alkyl spacer length, highlighting the negative impact of the excessive water uptake on operational stability.

Additionally, adding salt has emerged as an effective way to improve operational stability. Anthopoulos and Inal *et al.* conducted experiments utilizing tetra-*n*-butylammonium fluoride (TBAF), an ammonium salt, as a dopant for n-type polymer P-90 (Fig. 3d).[96] The addition of TBAF was found to have dual benefits as both a molecular dopant and a morphology additive, resulting in notable enhancements in both performance and cycling stability. Specifically, the introduction of TBAF doping enabled the injection of electron charge carriers, effectively filling the trap states within P-90. This method minimized the trapping and de-trapping processes during device operation and electrochemical doping, contributing to enhanced stability. The OECTs based on TBAF(40 mol%)-doped P-90 exhibited remarkable cycling stability with stable transfer characteristics observed after 4.5 hours of cycling (810 cycles). Furthermore, the operational stability and shelf life of another n-type polymer P75-based OECTs have also been enhanced through the addition of salts such as tetrabutylammonium perchlorate, tetrabutylammonium hexafluorophosphate, and lithium perchlorate to the solution.[71] The authors proposed that these salts enhanced the porosity of the membrane, leading to better operational stability.

Processing optimization is also a practical and straightforward approach to enhancing the operational stability of n-type materials. Yue *et al.* enhanced the stability and performance of n-type small-molecule gNR (Fig. 5d) by using fluorinated alcohols (FAs) as the processing solvents.[85] They found that 2,2,2-trifluoroethanol (TFE), 1,1,1,3,3,3-hexafluoroisopropanol (HFIP), and perfluoro-*tert*-butanol (PFTB) showed up to 10 times better drain current stability (63.9% for TFE, 61.6% for HFIP, and 75.2% for PFTB) than chloroform (7.3%) after 600 times cycling. This enhancement is due to optimized molecular packing that effectively prevents the penetration and degradation caused by oxygen and water. A similar strategy was also used for another

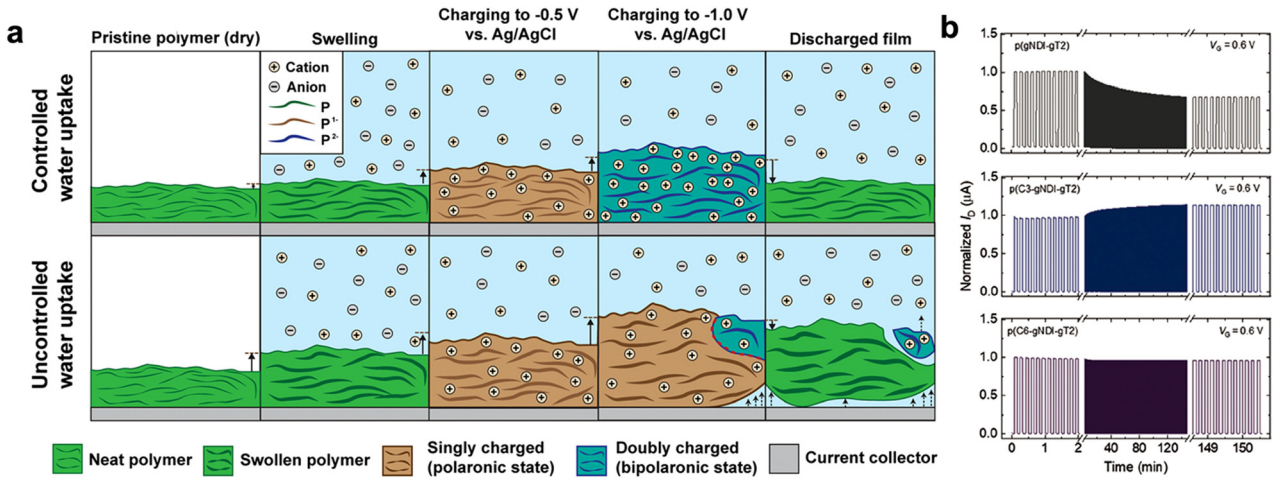

Fig. 6 The negative impact of excessive water uptake on operational stability. (a) Illustration of the charging mechanism of redox-active polymers with controlled water uptake and uncontrolled water uptake. Reprinted with permission from ref. 41. Copyright 2022, Nelson and Giovannitti *et al.* Published by American Chemical Society. This publication is licensed under CC-BY 4.0. (b) Stability pulsing measurements with alternating gate potentials between V_G = 0 and 0.6 V for p(gNDI-gT2), p(C3-gNDI-gT2), and p(C6-gNDI-gT2) for OECT channels biased at V_D = 0.6 V in a 0.1 M NaCl aqueous solution under ambient conditions. Reprinted with permission from ref. 74. Copyright 2021, Maria and Giovannitti *et al.* Published by Wiley-VCH GmbH, Weinheim. This publication is licensed under CC-BY 4.0.

n-type small-molecule, 4Cl-PDI-4EG (Fig. 5b). When processed with HFIP as the solvent, no decrease in drain current was observed for over 1 hour of cycling (600 cycles).[83] Although several methods have been proven effective for enhancing the stability of n-type materials, the long-term operational stability of many high-performance n-type OECT materials is still poor. Thus, further study on the origin and mechanism of the stability issue is needed.

4 Applications of n-type and ambipolar OECTs

Currently, the majority of applications utilizing OECTs rely solely on p-type OECTs. These applications include chem/biosensing, electrophysiological recording, and neuromorphic computing. The primary reason for this is the scarcity of reliable and high-performing n-type and ambipolar OECT materials.[17] However, with the fast development of n-type and ambipolar OECT materials, exciting new features and applications have emerged. These include constructing complementary logic circuits,[27,97] enhanced electrophysiological recording, high-sensitivity electrochemical biosensing,[30] and versatile neuromorphic simulation.[89,98]

4.1 Complementary logic circuits

Complementary logic circuits are a form of digital logic design that leverages complementary pairs of n-type and p-type transistors. These circuits offer many benefits, including high gain, low static power consumption, fast switching times, and compatibility with existing electronic devices.[99] They serve as the foundation for various logic gates and digital circuits, which can be implemented using different transistor technologies.[100] One widely used technology is complementary metal-oxide-semiconductor, which has been widely used in integrated circuit design for various digital logic and analog circuits in modern electronics. The development of OECT-based complementary circuits holds great significance in developing more functions and applications of OECTs. In a complementary inverter, an n-type transistor is connected in parallel with a p-type transistor (Fig. 7a), with their drains connected to the output, and their gates connected to the input. In addition, the sources of n-type and p-type transistors are connected to the ground (GND) and the supply voltage (V_{DD}) respectively. When the input voltage is close to zero, the p-type transistor conducts while the n-type transistor is cut off. As a result, the output voltage equals V_{DD}. As the input voltage increases and approaches V_{DD}, the p-type transistor is cut off, and the n-type transistor operates in a linear regime. Consequently, the output voltage approaches the GND.

The relevant parameters to evaluate inverters are the voltage transfer characteristic (VTC), operating voltage (V_{DD}), noise margin (NM), power consumption, and switching frequency. The VTC shows the relationship between the input voltage (V_i) and the output voltage (V_0) of the inverter. The static gain is calculated as:

$$\text{Gain} = dV_0/dV_i \quad (3)$$

Typically, the maximum gain is achieved by selecting an appropriate voltage step size, as the value of G strongly depends on the input voltage step size used for measurement.[101] Power consumption is another important parameter that includes static and dynamic power consumption (P_S, P_D). P_S can be ignored in a typical complementary circuit by using enhancement-mode transistors, due to their neglecting static current. However, P_D is mainly produced by charging and discharging the capacitor during the switching process. The average P_D can be explained as:

$$P_{D,AVG} = C_L V_{DD}^2 f \quad (4)$$

where C_L is the load capacitance and f is the operating frequency. Hence, by reducing either the C_L or V_{DD}, the average dynamic power consumption can be effectively reduced at the same operating frequency. Furthermore, the NM is a critical metric for evaluating the reliable and robust operation of a logic circuit. A higher noise margin indicates a more reliable circuit with improved tolerance to noise. In inverter circuits, two logic values, "0" and "1" are defined, resulting in two corresponding noise margins. The NM in the "low" state (or "high" state) is expressed as $NM_L = V_{IL} - V_{OL}$ (or $NM_H = V_{OH} - V_{IH}$), where V_{IL} (or V_{OH}) is the maximum input (or output) low voltage and V_{OL} (or V_{IH}) is the minimum output (or input) high voltage. The most common definition method for V_{OL} and V_{IL} (or V_{OL} and V_{IH}) is the point on the transfer curve with a slope of -1 when transitioning from high level to low level (or from low level to high level).[102] The NM can reach its maximum value of $(V_{DD} - GND)/2$ when the inverter's transfer characteristic exhibits a sharp transition from V_{DD} to GND and the switching voltage is ideally positioned at $V_{DD}/2$. This can be accomplished by employing both n-type and p-type transistors with similar properties, including threshold voltage and performance characteristics.[101] This balanced configuration ensures consistent and symmetrical performance, leading to improved signal integrity, enhanced noise immunity, and reduced distortion.

Inverters can also be constructed using ambipolar or unipolar materials. Ambipolar inverters share the same structure as complementary inverters but offer the advantage of simplified processing methods and increased integration density.[19] However, ambipolar transistors, which cannot completely turn off at the zero bias, limit the voltage adjustment range and result in reduced gain and NM, as well as non-negligible energy loss in both the "0" and "1" states (Fig. 7b). Furthermore, unipolar inverters can be made by connecting two transistors with the same polarity in series. This can be achieved using the "zero-V_{GS}" or "diode-load" configuration (Fig. 7(c) and (d)). The diode-load inverter provides limited gain while the zero-V_{GS} inverter with larger gain but requires both enhancement mode and depletion mode transistors (*e.g.*, the top one is a p-type accumulation-mode transistor and the bottom one is a p-type depletion-mode transistor). Besides, the zero-V_{GS} inverter has a non-negligible static power consumption in the state "1" and lower NM. Compared to complementary inverters, both unipolar zero-V_{GS} inverters and ambipolar inverters offer similar gains, but they come with significant static power dissipation and reduced NM. Thus, it is crucial to create n-type materials that possess voltage and performance properties similar to p-type materials.

4.2 Applications of complementary logic circuits

Using BBL as the n-channel material and the p-type polymer P3CPT (Fig. 9b), the first OECT complementary logic circuit with a gain of 11 (Table 4) was realized by Fabiano *et al.*[17] Later, they developed an alcohol-dispersed n-type conductive ink by doping BBL with poly(ethyleneimine) (PEI).[48] The resulting BBL:PEI films exhibited a high electrical conductivity of 8 S cm^{-1} and also displayed excellent ambient stability, leading to the first depletion mode n-type OECT. Additionally, the combination of the n-type BBL:PEI and the p-type PEDOT:PSS (Fig. 9a), both of which operate in the depletion mode, led to the realization of ternary logic gates. Ternary logic gates are a class of digital logic gates capable of processing three distinct input states and generating three different output states. The

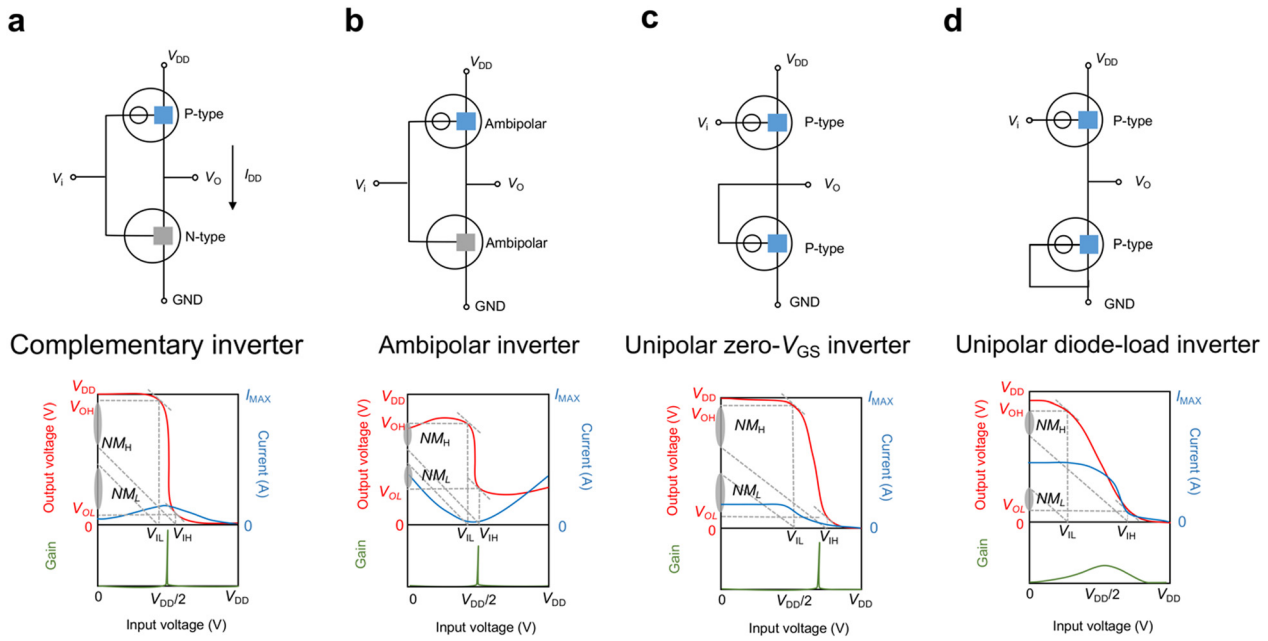

Fig. 7 Typical circuit diagrams and VTCs of inverters constructed by (a) both n-type and p-type materials, (b) single ambipolar material, (c) single p-type material in a "zero-V_{GS}" configuration and (d) single p-type material in a "diode-load" configuration. In the VTCs, gain, noise margin (NM) and I_{DD} current flowing from V_{DD} to GND are labeled.

Table 4 Summary of the performance characteristics of complementary circuits-based OECTs

Materials	Transporting type	Gain (V/V)	V_{DD} (V)	NM (V)	P_S[c] and P_D[c] (μW)	Ref.
BBL	n	11	0.6	0.2	—	17
P3CPT	p					
BBL:PEI[a]	n	6	−0.07, 0.38		—, <10	48
PEDOT:PSS[a]	p					
BBL:MWCNT(10 : 1)	n	16	0.6	—	0.04, <1	90
PEDOT:PSS	p					
BBL_{152}	n	100	0.7	85%[b]	0.78×10^{-3}, <2.2	68
P($g_4$2T-TT)	p					
BBL	n	33	0.7	—	—	97
P($g_4$2T-TT)	p					
Homo-gDPP:Cin-Cell	n	150	0.7	—	—	27
gDPP-g2T:Cin-Cell	p					
P(gTDPP2FT)	n	26	0.8	—	—	14
P(gTDPPT)	p					
PrC60MA:P(g2T-TT)95 : 5(w:w)	n and p	82, 62	0.9, −0.8	—	—	18
2DPP-OD-TEG	n and p	50	1.4	—	—	15
BBL:PBBTL	n and p	31, 42	0.6, −0.6	—	—	69
p(C_4-T2-C_0-EG)	n and p	28	0.8	—	57.7×10^{-3}, —	75

Means the data are missing in the literature. [a] The data are extracted from OECT-based ternary logic gates. [b] The NM is expressed as a percentage of V_{DD}. [c] The static power (P_S) and dynamic power (P_D) are extracted at the maximum gain.

resulting logic gates exhibited gains of up to 6.[48] Furthermore, using BBLs with higher molecular weights and the p-type polymer P($g_4$2T-T) (Fig. 9c), the inverter gain reached an impressive value of up to 100 with a P_D of 2.2 μW.[67]

In previous studies, because the performance of n-type and p-type materials was largely different and there was lack of a good method for OECT material patterning, many studies used separate substrates to construct an inverter. In 2022, Lei *et al.* reported an n-type polymer P(gTDPP2FT) (Fig. 4d) with high performance. They successfully integrated this n-type material with a compatible p-type material P(gTDPPT) to create a single-substrate inverter. The inverter exhibited a high gain of 26 (Table 4).[14] Using ambipolar materials presents a potential solution for simplifying the device fabrication process. One example is using 2DPP-OD-TEG (Fig. 5e) to create logic circuits, including inverters, NAND gates, and NOR gates.[15] Blend-based ambipolar materials such as p(g2T-TT) with PrC60MA (Fig. 5h) or BBL with PBBTL polymers (Fig. 5i), also enable the construction of high-performance OECT logic circuits.[18,69]

Device structure innovation can reduce the device size of an inverter. In 2021, Rivnay *et al.* introduced a vertical-OECT (vOECT) architecture for ambipolar OECTs, which utilizes a device structure instead of the conventional planar two-dimensional structure (Fig. 8c). The advantage of vOECT is that the length is defined by the thickness between the two electrodes, and an nm-controllable channel length can be achieved, thereby leading to high transconductance, which is difficult to achieve in a planar structure using regular photolithography. vOECT-based complementary logic circuits are realized by combining two coplanar vertical structures and utilizing ambipolar materials as the channel materials. When using ambipolar polymer p(C4-T2-C_0-EG) (Fig. 5f), as the channel material, the vOECT-based inverter achieved a high gain of 10 (Table 4).[19] The adoption of vOECT enables the retention of high gain while reducing the footprint per inverter by 50%, but it faces limitations in utilizing ambipolar materials and increased fabrication challenges.

Very recently Huang, Zheng, Cheng, J. Marks and Facchetti *et al.* reported the first vertically stacked OECTs (vsOECTs) and their logic circuits.[27] Different from previously reported vOECTs, vsOECTs were created by spin-coating the semiconductor onto the bottom Au source electrode and then evaporating the top intersecting Au drain electrode (Fig. 8a). Additionally, vsOECTs-based inverters can be achieved by placing the n-type vsOECTs directly on top of the p-type vsOECTs. The redox-active p-type (gDPP-g2T) and n-type (Homo-gDPP) (Fig. 9f) semiconducting polymers blended with a redox-inert and photocurable polymer component (cinnamate-cellulose polymer (Cin-Cell, Fig. 9d)), respectively, and then used as the OECT channel material. Cin-Cell functions as a structural stabilizer for OECTs, resulting in enhanced stability of the semiconducting polymer. The gDPP-g2T:Cin-Cell and Homo-gDPP:Cin-Cell blends show almost no current drop after 50 000 cycles, while the non-blended polymer drops to the off state after 5 cycles. This inverter based on these high-stability polymers exhibited a sharp voltage transition with a gain of around 150 (Table 4) and remained stable for over 30 000 switching cycles. Moreover, vsOECT has demonstrated its ability to fabricate complex electronic devices such as NAND, NOR logic gates, and rectifiers (Fig. 8b).

Apart from the ongoing miniaturization of OECT-based inverters, the advancement of large-area processing technology is also noteworthy. This is particularly important as conventional photolithography techniques have limitations in terms of scalable and large-area fabrication. In 2022, Fabiano *et al.* successfully demonstrated large-area OECT-based inverters by using screen-printing and spray-coating techniques.[97] P-type P($g_4$2T-T) (Fig. 9c) and n-type BBL (Fig. 3a) were dispersed in alcohol solvents in the form of nanoparticle inks for large-scale printing. Moreover, poly(sodium-4-styrene sulfonate) (PSSNa) and polyquaternium-10 (PQ-10)-based hydrogels were chosen as the printable electrolyte for the n-channel OECT and the p-channel OECT, respectively. The resulting printed OECTs' logic circuits realized a maximum gain value of 193 (V/V) (Table 4) by cascading two single-stage inverters.

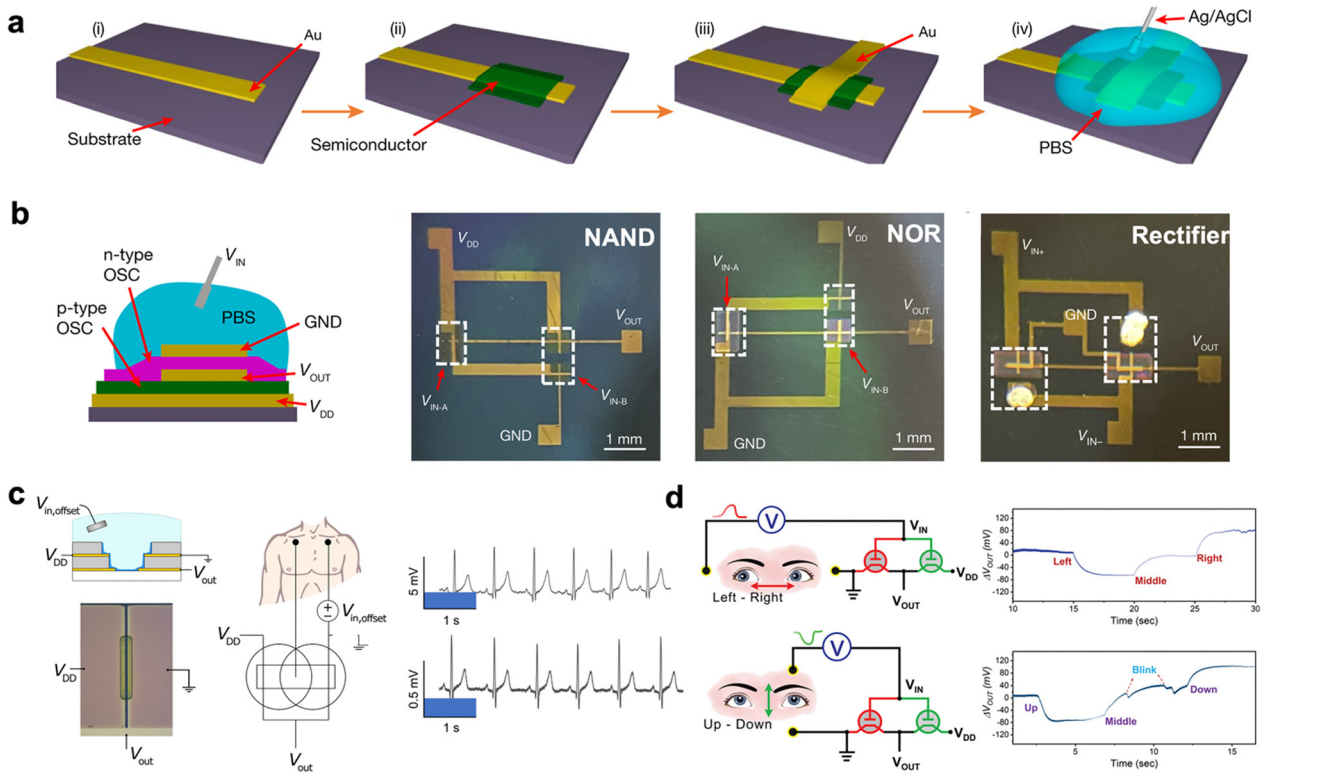

Fig. 8 Complementary circuits and their applications in electrophysiological recording. (a) The fabrication process for vsOECTs: (i) thermal evaporation of the bottom source electrode with a shadow mask, (ii) spin-coating and photopatterning of the semiconducting polymer, (iii) thermal evaporation of the top drain electrode with a shadow mask and (iv) application of a phosphate buffer solution (PBS) electrolyte and Ag/AgCl gate electrode. (b) Illustration of vsOECT-based inverters and photographs of NAND, NOR circuits, and rectifier. Reprinted with permission from ref. 27. Copyright 2023, Huang, Zheng, Cheng, Marks and Facchetti *et al.* Published by Springer Nature. This publication is licensed under CC-BY 4.0. (c) Schematic diagram of a coplanar inverter based on vOECT (left) and its application in ECG signal amplification: the operational principle (middle), the ECG signal recorded from the output of the vOECT-based inverter (top) and the ECG signal recorded directly between the adhesive medical electrodes (bottom). Reprinted with permission from ref. 19. Copyright 2021, Rivnay *et al.* Published by American Association for the Advancement of Science (AAAS). This publication is licensed under CC-BY 4.0. (d) EOG signals monitored by complementary circuits including the operational principle and results for left–right eye movement (top) and up–down eye movements (bottom). Reprinted with permission from ref. 69. Copyright 2022, Wiley-VCH GmbH.

The performance characteristics of all reported complementary circuit-based OECTs are summarized in Table 4.

These achievements in logic circuits not only laid the foundation for amplifying weak voltage signals but also made integrated production and large-area manufacturing possible. Complementary logic circuits have already offered benefits in enhanced electrophysiological recording, high-sensitivity ion monitoring, and multifunctional neuromorphic simulation. For instance, the inverters based on ambipolar material BBL:PBBTL blends realize tracking of eye movement when the eyes blink signals at frequencies higher than 1 Hz (Fig. 8d).[69] Additionally, the vOECT-based inverters, using ambipolar material p(C_4-T2-C_0-EG) as the channel, enable the recording of electrocardiograms from healthy participants with a gain of 10 (Fig. 8c). Furthermore, Torricelli *et al.* developed an ion-sensing inverter using p-type PEDOT:PSS and n-type BBL. The sensor showed excellent linearity from 10^{-5} M to 1 M for K^+ and displayed an impressive sensitivity of up to 1172 mV dec^{-1} with a low supply voltage of 0.5 V.[24] The normalized voltage sensitivity achieved in this study exceeds 2300 mV V^{-1} dec^{-1}, which is two orders of magnitude higher than previous studies utilizing a single p-type transistor.[103,104]

Artificial synapses constructed using electronic devices are important for neuromorphic computing. These devices can address the limitations of traditional CMOS-based computing, overcoming the von-Neumann bottleneck and providing potential solutions for the post-Moore's law era.[105] Compared to MOSFETs and other ion-impermeable transistors, OECTs offer several advantages, including high transconductance, improved biocompatibility, and reduced mechanical mismatch with biological tissues. In recent years, p-type-based OECTs have demonstrated their potential in simulating basic synaptic functions, such as spiking rate-dependent plasticity, paired-pulse facilitation, and long-term plasticity.[26] However, the absence of n-type or ambipolar materials poses a limitation on the creation of more artificial neuron functions. Recently, Fabiano *et al.* reported the concept of organic electrochemical neurons (OECNs). They developed all-printed complementary OECTs based on BBL and a p-type polymer, P($g_4$2T-T) (Fig. 9c) and created OECNs that closely mimic the firing of nerve pulses through ion-based mechanisms similar to those found in biological systems (Fig. 10a).[25] OECNs, when connected with a single synaptic transistor enabled the integration of a neuro-synaptic system, demonstrating the concept of

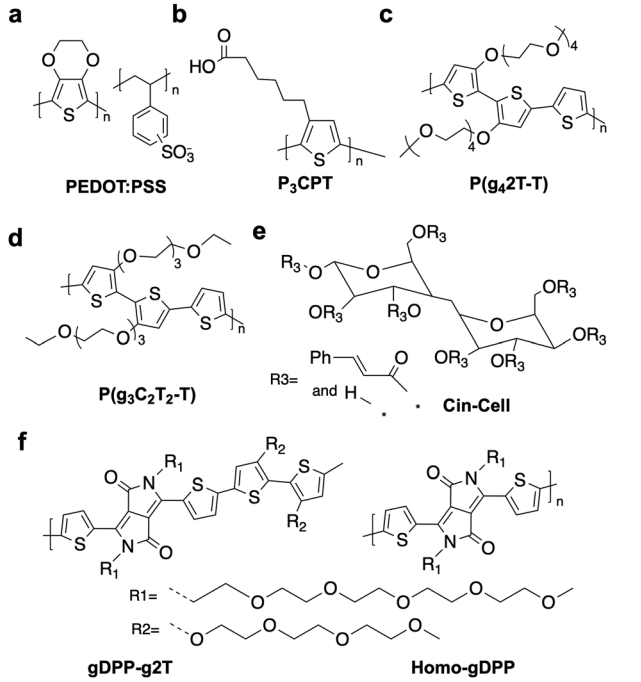

Fig. 9 Chemical structures of the (a)–(d) p-type polymers, (e) and (f) redox-active polymers utilized in building OECT-based inverters.

'neurons which fire together wire together'. This organic electrochemical neuro-synaptic system is an important step, capable of creating more complex sensory and processing systems with learning capabilities (Fig. 10a).

Very recently, they introduced a bio-realistic conductance-based organic electrochemical neuron (C-OECN)[23] based on the Hodgkin-generation and propagation of electrical signals in neurons since its formulation in 1952. The remarkable stable anti-ambipolar properties of BBL were discovered and utilized in both the Na^+-based and K^+-based OECT channels of C-OECN. C-OECN is capable of spiking at bio-plausible frequencies of nearly 100 Hz, faithfully emulating key biological neural characteristics and enabling ion-based spiking modulation (Fig. 10b). By coupling C-OECN with a mouse's right cervical vagus nerve, the circuit demonstrated the ability to respond to specific concentrations of biochemical signals by modulating voltages within the circuit.

4.3 Biological sensing

Biological sensing is important in expanding our knowledge of living systems, enhancing healthcare methodologies, discovering new therapies, and tackling diverse challenges in biology, medicine, and environmental sciences. The emergence of bioelectronics, which bridges the gap between electronics and biology, has sparked significant interest in the development of innovative biomedical devices for disease diagnosis and treatment. OECTs have shown great potential in detecting various biomolecules such as enzymes, cortisol, immune response molecules, metabolites, *etc.* PEDOT:PSS (Fig. 9a) was often used in OECT-based sensing.[106,107] It is a commercially available polymer that offers outstanding characteristics such as high electrical conductivity, ion modulation, and good biocompatibility.[108] Notably, PEDOT:PSS works in depletion mode, leading to increased static power consumption that restricts its integration potential. N-Type accumulation OECT-based sensors provide advantages like reduced power consumption and improved sensitivity, due to their effective electron transport and ability to operate with negative voltages.

Inal *et al.* employed an n-type polymer, P-90 (Fig. 3d), in conjunction with lactate oxidase (LOx) for enzymatic sensing of lactate. When lactate was oxidized by the enzyme, electrons were released that were directly captured by the polymer. This results in a rapid and sensitive response in terms of current output.[29] In addition, n-type materials exhibit a progressive current increase, in contrast to the declining current observed in p-type materials, enabling better discrimination of smaller currents. The device exhibited a specific and reversible response to lactate, with a detection limit of 10 μM. This work represents the first utilization of an accumulation mode OECT for biological sensing, paving the way for n-type materials with enhanced sensitivity and lower power consumption. Later on, this method was utilized for glucose detection and the competition process between polymer and oxygen for electrons was analyzed. When glucose's concentration is low, oxygen outcompetes the polymer and acquires electrons, producing hydrogen peroxide in the channel. This leads to a gradual increase in current. As oxygen becomes depleted, the polymer directly receives electrons, leading to a substantial increase in current. This showcases the improved sensitivity achieved by the n-type material's capability to stabilize electrons (Fig. 11a). The device exhibits a low detection limit of 10 nM and an impressive dynamic range spanning over 8 orders of magnitude.[28]

Subsequently, by combining p-90 and glucose oxidase (GOx) an OECT platform with microfluidic channels, real-time monitoring with high transconductance and an impressive detection limit as low as 1 nM was achieved.[21] Recently, the influence of the thin film surface properties on the performance of metabolite sensors was investigated using n-type materials with different side chains. The sensors' performance is closely related to the orientation of the enzyme on the polymer surface, which can be adjusted by the surface charge. When the surface carries a negative charge, it encourages the enzyme to adopt an optimal orientation for effective catalysis.[20] In addition, the potential of using enzymatic fuel cells for self-powered sensors was also explored. A glucose-fueled power supply was developed utilizing a GOx-adsorbed P-90 anode and an organic cathode p(EDOT-*co*-EDOTOH) (Fig. 11b). The system demonstrated maximum power density when supplied with 10 mM glucose, generating sufficient power to operate an OECT device.[23] This innovative approach opens up new possibilities for self-powered biosensors.

Further notable progress is the integration of a micron-scale OECT with a microfluidic platform, enabling label-free detection of Aβ aggregates in human serum. This work used a nanoporous membrane functionalized with Congo red (CR) molecules, which has been proven to have a strong affinity for Aβ aggregates in a previous study. As CR units capture Aβ aggregates, the Aβ binding increases the overall capacitance and amplifies the

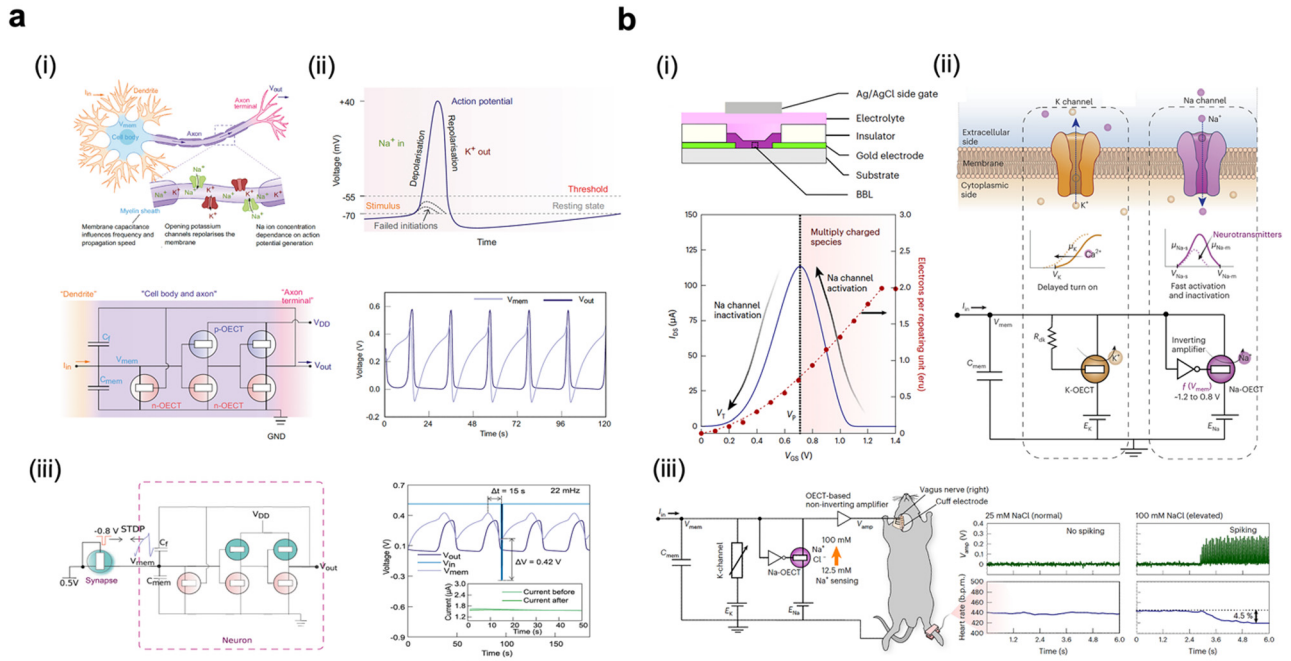

Fig. 10 The applications in neuromorphic simulation. (a) Organic electrochemical neurons based on an axon hillock circuit. (i) Schematic of a biological neuron and its analogy with the organic electrochemical neuron based on an axon hillock circuit. (ii) Different phases of the action potential in a nerve cell and spiking behaviors of the organic electrochemical neurons. (iii) Schematic showing the integration of a neuro-synaptic system and the change in synaptic conductivity and the resulting change in frequency of the neuron. Reprinted with permission from ref. 25. Copyright 2022, Fabiano *et al.* Published by Springer Nature. This publication is licensed under CC-BY 4.0. (b) Conductance-based organic electrochemical neuron based on a Hodgkin–Huxley circuit. (i) Structure of an OECT device and antiambipolar behavior in BBL resembling activation and inactivation of sodium channels in a neuron. (ii) Conductance-based organic electrochemical neuron based on a Hodgkin–Huxley circuit and analogy with the biological neurons with Na^+ and K^+ channels. (iii) The c-OECN circuit showing Na-OECT and integration with the vagus nerve and its ability to sense biochemical signals. Reprinted with permission from ref. 23. Copyright 2022, Fabiano *et al.* Published by Springer Nature. This publication is licensed under CC-BY 4.0.

electrical field imposed on the channel. Three polymers have been used as channels, including p-type depletion PEDOT:PSS, p-type accumulation p(g0T2-g0T6), and n-type accumulation p(C_6NDI-T) (Fig. 3h). As a result, the n-type OECT device demonstrates the capability to detect a wide concentration range spanning over 8 orders of magnitude, using a mere 1 μL of human serum sample, exhibiting increased sensitivity over p-type materials. This is due to the behavior of positively charged Aβ accumulating on the functionalized membrane, repelling more cations into the channel and thus improving the detection sensitivity of n-type materials channel-doped by cations. On the contrary, it attracts anions and causes a decrease in the detection sensitivity of p-type materials.[21] Moreover, a lower power demand has been achieved for n-type accumulation-mode devices (power consumption in PBS is 0.29 mW) for PEDOT:PSS, 0.21 mW for p(g0T2-g6T2) and 0.057 μW for p(C_6NDI-T) (Fig. 11d).

In 2022, Inal *et al.* reported OECT-based immunosensors for the rapid and accurate detection of SARS-CoV-2 spike proteins. These novel devices incorporate alternating current electrothermal flow, ensuring swift and precise analyte delivery to the sensor surface, resulting in ultra-fast response times. The OECT employs both p-type p(g_3C_2T2-T) (Fig. 9e) and n-type p(C_6NDI-T) (Fig. 3h) as channel materials. Although the p-type OECT outperforms the n-type in terms of transconductance (g_m: 60 mS *vs.* g_m: 15 μS), when it is operated using the same biofunctionalized gates, the detection limit of the n-type device is as low as 100×10^{-18} M, three orders of magnitude lower than the state-of-the-art p-type material. This remarkable enhancement in detection sensitivity can be attributed to the n-type material's ability to achieve a closer equivalent capacitance between the gate and the channel ($C_{channel} \approx C_{gate}$).[22] Consequently, the change in gate capacitance during the detection process leads to a larger voltage drop in the channel compared to the p-type material.

5 Conclusions and outlook

In the past several years, significant progress has been made in the development of n-type and ambipolar OECT materials and applications. Although OECTs share a similar device structure with OFET devices, recent studies have demonstrated that conventional molecular design strategies used in high-performance OFETs might not fit well with OECTs, since OECTs work under heavily doped states in water and have a bulk doping feature. We would like to highlight several material design strategies: (1) a side-chain-free design that makes polymers with high volumetric capacitance; (2) apart from designing polymers with low-lying LUMO energy levels, considering the "doped state" properties of

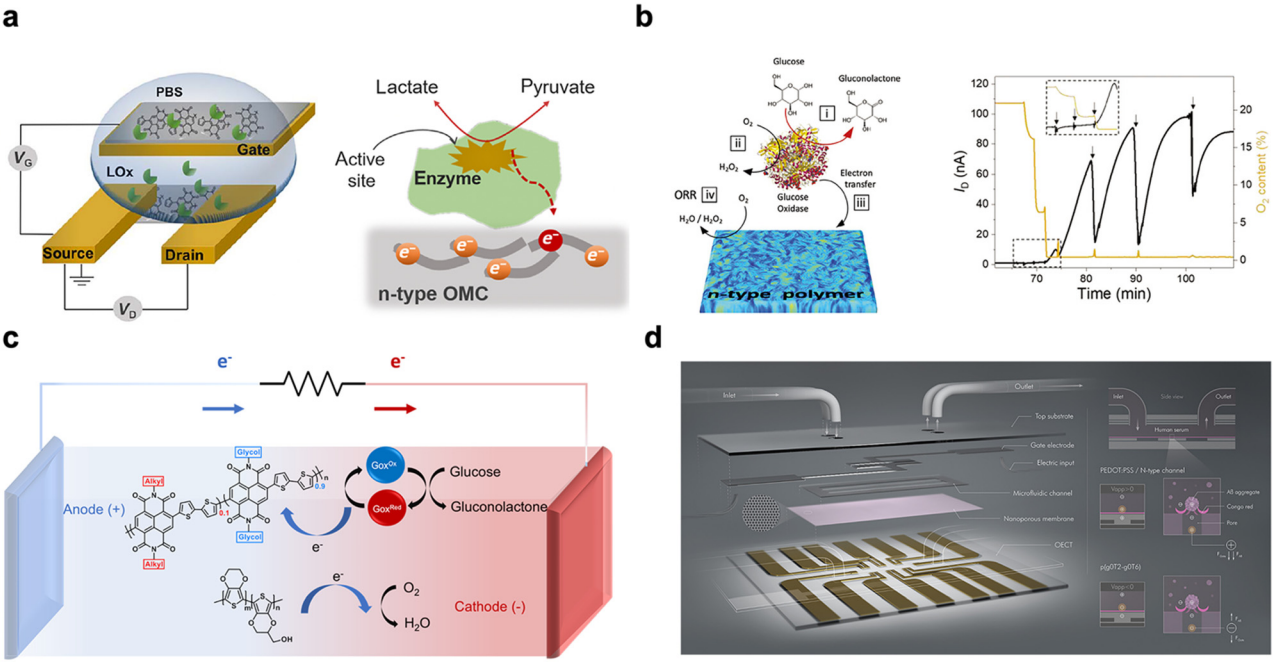

Fig. 11 Biological sensing based on n-type OECT materials. (a) Schematic of an OECT biosensor and the mechanism of lactate sensing based on the direct electron transfer from the enzyme to the n-type organic semiconductors. Reprinted with permission from ref. 29. Copyright 2018, Inal and M. Owens *et al.* Published by AAAS. This publication is licensed under CC-BY 4.0. (b) P-90/GOx-based sensor for glucose, with an illustration of the corresponding glucose oxidation and transfer of electrons to the n-type channel and the real-time current response of the n-OECT sensor, as successive glucose solutions were added to PBS. Reprinted with permission from ref. 28. Copyright 2022, Wiley-VCH GmbH. (c) Schematic of membrane-free fuel cells. The fuel cells comprise P-90/GOx at the anode and p(EDOT-*co*-EDOTOH) at the cathode and reactions that occur during the operation of the fuel cells.[30] (d) Schematic of the μf-OECT for Aβ detection (left panel) and the sensor operation principle. The positively charged Aβ aggregates captured by the Congo red molecules of the membrane modulate the gate voltage imposed on the channel. (right panel). Reprinted with permission from ref. 21. Copyright 2022, Inal *et al.* Published by American Chemical Society. This publication is licensed under CC-BY 4.0.

polymers is also essential; (3) because small molecule packings can be easily distorted by ion injection/diffusion, constructing supramolecular polymers or oligomers provides a viable approach for high-performance small-molecule OECTs; and (4) for ambipolar materials, blending p- and n-type materials is a simple and general approach but needs further in-depth study. Besides, the stability issue in OECT materials is also critical for their practical applications. Various approaches have been identified to enhance the operational stability including (1) side-chain engineering to mitigate excessive water absorption, (2) incorporating dopants or salts, and (3) optimizing molecular packings *via* process engineering, *etc.*

To further enhance the performance of n-type and ambipolar OECT materials, we believe that the following three questions need careful consideration. Firstly, unlike OFET materials, OECT materials operate in a highly doped state in aqueous media. What factors determine the materials' performance? Secondly, most OECT polymers use ethylene glycol (EG) side chains. Are EG side chains the optimal choice? Thirdly, side-chain-free polymers show promise as they lack "insulating" and "electrochemically inert" side chains. Are they a new research direction for OECT materials? For the above questions, our answers are as follows: (1) our preliminary study on the "doped state" of conjugated polymers suggests that OECT materials design is similar to but distinct from OFETs.[14] Apart from their properties in the "neutral state", the properties of OECT materials in the "doped state" also require careful consideration. (2) Currently, EG side chains are the best, because they exhibit good ion transport features not only in OECTs but also in other fields, such as battery electrolytes. However, we think that other hydrophilic side chains (*e.g.* ionic side chains or side chains with functional groups) are also worth investigating as they may impart additional features to the polymers (*e.g.* biological functions). (3) Side-chain-free polymers indeed deserve further research. For example, BBL demonstrates both excellent performance and outstanding stability, and PBFDO has shown remarkable advantages in terms of μC^* in thin films. However, side-chain-free polymers have several drawbacks. They typically have limited chemical structures with low solubility in common solvents, making large-area solution processing challenging. In addition, in p-type polymers, the current state-of-the-art polymers are still thiophene polymers with suitable EG chains.[109] Side-chain-free polymers have not shown significant advantages.

Apart from n-type and ambipolar materials study, increasing interest has been devoted to exploring the new applications and features of OECT circuits, including enhanced electrophysiological recording, multifunctional artificial synapse simulation, and highly sensitive biosensing. We would like to highlight several important advancements: (1) n-type OECTs exhibited superior sensitivity, specifically in enzyme-catalyzed sensing,

probably due to their efficient electron transport; (2) "vertical" OECT structures with ambipolar materials can result in a 50% reduction of the logic circuit size, promising miniaturized biosensors (*e.g.* sensors for single neurons);[110] and (3) many behaviors of OECTs are similar to neurons, and neuron-like devices are an attractive research direction.

Despite these advancements, several challenges remain. First, the performance and operational stability of both n-type and ambipolar materials still lag behind their p-type counterparts. Second, it seems that LUMO energy levels have little correlation with the performance and stability of n-type OECTs, and establishing a clear structure–performance relationship is necessary. Third, OECTs have shown more and more interesting applications, especially in bioelectronics and biomimicking devices. Thus, exploring their new applications is exciting. Additionally, it is necessary to focus more on the development of ambipolar materials, considering their potential contributions to the field. We anticipate more substantial progress in the next few years, including more high-performance OECT materials and devices, exciting new applications, and their practical applications in flexible and wearable electronics.

Conflicts of interest

The authors have no conflicts of interest to declare.

Acknowledgements

This work was supported by the Beijing Natural Science Foundation (JQ22006) and the King Abdullah University of Science and Technology Research Funding (KRF) under Award No. ORA-2021-CRG10-4668.4.

References

1 S. Griggs, A. Marks, H. Bristow and I. McCulloch, n-Type organic semiconducting polymers: stability limitations, design considerations and applications, *J. Mater. Chem. C*, 2021, **9**, 8099–8128.
2 E. Wang, W. Mammo and M. R. Andersson, 25th anniversary article: isoindigo-based polymers and small molecules for bulk heterojunction solar cells and field effect transistors, *Adv. Mater.*, 2014, **26**, 1801–1826.
3 J. Rivnay, S. Inal, A. Salleo, R. M. Owens, M. Berggren and G. G. Malliaras, Organic electrochemical transistors, *Nat. Rev. Mater.*, 2018, **3**, 1–14.
4 G. Horowitz, Organic field-effect transistors, *Adv. Mater.*, 1998, **10**, 365–377.
5 A. Marks, S. Griggs, N. Gasparini and M. Moser, Organic electrochemical transistors: an emerging technology for biosensing, *Adv. Mater. Interfaces*, 2022, **9**, 2102039.
6 Y. Zhong, A. Saleh and S. Inal, Decoding Electrophysiological Signals with Organic Electrochemical Transistors, *Macromol. Biosci.*, 2021, **21**, 2100187.
7 A. Nawaz, Q. Liu, W. L. Leong, K. E. Fairfull-Smith and P. Sonar, Organic electrochemical transistors for in vivo bioelectronics, *Adv. Mater.*, 2021, **33**, 2101874.
8 J. Perez and S. Shaheen, Neuromorphic-based Boolean and reversible logic circuits from organic electrochemical transistors, *MRS Bull.*, 2020, **45**, 649–654.
9 G. Malliaras and I. McCulloch, Introduction: Organic Bioelectronics, *Chem. Rev.*, 2022, **122**, 4323–4324.
10 B. Crone, A. Dodabalapur, Y.-Y. Lin, R. Filas, Z. Bao, A. LaDuca, R. Sarpeshkar, H. Katz and W. Li, Large-scale complementary integrated circuits based on organic transistors, *Nature*, 2000, **403**, 521–523.
11 J. Zaumseil and H. Sirringhaus, Electron and ambipolar transport in organic field-effect transistors, *Chem. Rev.*, 2007, **107**, 1296–1323.
12 H. Sun, J. Gerasimov, M. Berggren and S. Fabiano, n-Type organic electrochemical transistors: materials and challenges, *J. Mater. Chem. C*, 2018, **6**, 11778–11784.
13 M. Moser, T. C. Hidalgo, J. Surgailis, J. Gladisch, S. Ghosh, R. Sheelamanthula, Q. Thiburce, A. Giovannitti, A. Salleo and N. Gasparini, Side chain redistribution as a strategy to boost organic electrochemical transistor performance and stability, *Adv. Mater.*, 2020, **32**, 2002748.
14 P. Li, J. Shi, Y. Lei, Z. Huang and T. Lei, Switching p-type to high-performance n-type organic electrochemical transistors via doped state engineering, *Nat. Commun.*, 2022, **13**, 5970.
15 J. J. Samuel, A. Garudapalli, A. A. Mohapatra, C. Gangadharappa, S. Patil and N. P. B. Aetukuri, Single-Component CMOS-Like Logic using Diketopyrrolopyrrole-Based Ambipolar Organic Electrochemical Transistors, *Adv. Funct. Mater.*, 2021, **31**, 2102903.
16 H. Y. Wu, C. Y. Yang, Q. Li, N. Kolhe, X. Strakosas, M.-A. Stoeckel, Z. Wu, W. Jin, M. Savvakis, R. Kroon, D. Tu, H. Woo, M. Berggren, S. Jenekhe and S. Fabiano, Influence of Molecular Weight on the Organic Electrochemical Transistor Performance of Ladder-Type Conjugated Polymers, *Adv. Mater.*, 2021, **34**, 2106235.
17 H. Sun, M. Vagin, S. Wang, X. Crispin, R. Forchheimer, M. Berggren and S. Fabiano, Complementary logic circuits based on high-performance n-type organic electrochemical transistors, *Adv. Mater.*, 2018, **30**, 1704916.
18 E. Stein, O. Nahor, M. Stolov, V. Freger, I. M. Petruta, I. McCulloch and G. L. Frey, Ambipolar blend-based organic electrochemical transistors and inverters, *Nat. Commun.*, 2022, **13**, 5548.
19 R. B. Rashid, W. Du, S. Griggs, I. P. Maria, I. McCulloch and J. Rivnay, Ambipolar inverters based on cofacial vertical organic electrochemical transistor pairs for biosignal amplification, *Sci. Adv.*, 2021, **7**, eabh1055.
20 D. Ohayon, D. Renn, S. Wustoni, K. Guo, V. Druet, A. Hama, X. Chen, I. P. Maria, S. Singh, S. Griggs, B. C. Schroeder, M. Rueping, I. McCulloch and S. Inal, Interactions of Catalytic Enzymes with n-Type Polymers for High-Performance Metabolite Sensors, *ACS Appl. Mater. Interfaces*, 2023, **15**, 9726–9739.

21 A. Koklu, D. Ohayon, S. Wustoni, A. Hama, X. Chen, I. McCulloch and S. Inal, Microfluidics integrated n-type organic electrochemical transistor for metabolite sensing, *Sens. Actuators, B*, 2021, **329**, 129251.
22 A. Koklu, S. Wustoni, K. Guo, R. Silva, L. Salvigni, A. Hama, E. Diaz-Galicia, M. Moser, A. Marks and I. McCulloch, Convection Driven Ultrarapid Protein Detection via Nanobody-Functionalized Organic Electrochemical Transistors, *Adv. Mater.*, 2022, **34**, 2202972.
23 P. C. Harikesh, C.-Y. Yang, H.-Y. Wu, S. Zhang, M. J. Donahue, A. S. Caravaca, J.-D. Huang, P. S. Olofsson, M. Berggren, D. Tu and S. Fabiano, Ion-tunable antiambipolarity in mixed ion–electron conducting polymers enables biorealistic organic electrochemical neurons, *Nat. Mater.*, 2023, 1–7.
24 P. Romele, P. Gkoupidenis, D. A. Koutsouras, K. Lieberth, Z. M. Kovács-Vajna, P. W. Blom and F. Torricelli, Multiscale real time and high sensitivity ion detection with complementary organic electrochemical transistors amplifier, *Nat. Commun.*, 2020, **11**, 3743.
25 P. C. Harikesh, C.-Y. Yang, D. Tu, J. Y. Gerasimov, A. M. Dar, A. Armada-Moreira, M. Massetti, R. Kroon, D. Bliman, R. Olsson, E. Stavrinidou, M. Berggren and S. Fabiano, Organic electrochemical neurons and synapses with ion mediated spiking, *Nat. Commun.*, 2022, **13**, 901.
26 P. Gkoupidenis, N. Schaefer, B. Garlan and G. G. Malliaras, Neuromorphic functions in PEDOT: PSS organic electrochemical transistors, *Adv. Mater.*, 2015, **27**, 7176–7180.
27 W. Huang, J. Chen, Y. Yao, D. Zheng, X. Ji, L.-W. Feng, D. Moore, N. R. Glavin, M. Xie, Y. Chen, R. M. Pankow, A. Surendran, Z. Wang, Y. Xia, L. Bai, J. Rivnay, J. Ping, X. Guo, Y. Cheng, T. J. Marks and A. Facchetti, Vertical organic electrochemical transistors for complementary circuits, *Nature*, 2023, **613**, 496–502.
28 V. Druet, P. D. Nayak, A. Koklu, D. Ohayon, A. Hama, X. Chen, M. Moser, I. McCulloch and S. Inal, Operation Mechanism of n-Type Organic Electronic Metabolite Sensors, *Adv. Electron. Mater.*, 2022, **8**, 2200065.
29 A. M. Pappa, D. Ohayon, A. Giovannitti, I. P. Maria, A. Savva, I. Uguz, J. Rivnay, I. McCulloch, R. M. Owens and S. Inal, Direct metabolite detection with an n-type accumulation mode organic electrochemical transistor, *Sci. Adv.*, 2018, **4**, eaat0911.
30 D. Ohayon, G. Nikiforidis, A. Savva, A. Giugni, S. Wustoni, T. Palanisamy, X. Chen, I. P. Maria, E. Di Fabrizio, P. M. F. J. Costa, I. McCulloch and S. Inal, Biofuel powered glucose detection in bodily fluids with an n-type conjugated polymer, *Nat. Mater.*, 2020, **19**, 456–463.
31 H. Tang, Y. Liang, C. Liu, Z. Hu, Y. Deng, H. Guo, Z. Yu, A. Song, H. Zhao, D. Zhao, Y. Zhang, X. Guo, J. Pei, Y. Ma, Y. Cao and F. Huang, A solution-processed n-type conducting polymer with ultrahigh conductivity, *Nature*, 2022, **611**, 271–277.
32 Y. Yu, G. Zhu, L. Lan, J. Chen, X. Zhu, J. Duan, S. Cong, Z. Li, Y. Wang, Z. Wang, I. McCulloch and W. Yue, n-Type Glycolated Imide-Fused Polycyclic Aromatic Hydrocarbons with High Capacity for Liquid/Solid-Electrolyte-based Electrochemical Devices, *Adv. Funct. Mater.*, 2023, 2300012.
33 K. K. Liu, P. Li, Y. Lei, Z. Zhang, X. Pan, S. K. So and T. Lei, J-Type Self-Assembled Supramolecular Polymers for High-Performance and Fast-Response n-Type Organic Electrochemical Transistors, *Adv. Funct. Mater.*, 2023, 2300049.
34 A. Giovannitti, C. B. Nielsen, D.-T. Sbircea, S. Inal, M. Donahue, M. R. Niazi, D. A. Hanifi, A. Amassian, G. G. Malliaras and J. Rivnay, N-type organic electrochemical transistors with stability in water, *Nat. Commun.*, 2016, **7**, 13066.
35 E. Zeglio and O. Inganäs, Active materials for organic electrochemical transistors, *Adv. Mater.*, 2018, **30**, 1800941.
36 E. W. Paul, A. J. Ricco and M. S. Wrighton, Resistance of polyaniline films as a function of electrochemical potential and the fabrication of polyaniline-based microelectronic devices, *J. Phys. Chem.*, 1985, **89**, 1441–1447.
37 D. A. Bernards and G. G. Malliaras, Steady-state and transient behavior of organic electrochemical transistors, *Adv. Funct. Mater.*, 2007, **17**, 3538–3544.
38 L. Zhang, L. Wang, S. He, C. Zhu, Z. Gong, Y. Zhang, J. Wang, L. Yu, K. Gao, X. Kang, Y. Song, G. Lu and H.-D. Yu, High-Performance Organic Electrochemical Transistor Based on Photo-annealed Plasmonic Gold Nanoparticle-Doped PEDOT:PSS, *ACS Appl. Mater. Interfaces*, 2023, **15**(2), 3224–3234.
39 G. Sych, P. Rannou, M. Jullien-Palletier, S. Sadki, Y. Bonnassieux and S. Sanaur, Impact of Charge Carrier Injection/Extraction Performances in Low-Dimension PEDOT:PSS Organic Electrochemical Transistors, *Adv. Electron. Mater.*, 2023, 2201067.
40 P. R. Paudel, M. Skowrons, D. Dahal, R. K. Radha Krishnan and B. Lüssem, The transient response of organic electrochemical transistors, *Adv. Theory Simul.*, 2022, **5**, 2100563.
41 A. A. Szumska, I. P. Maria, L. Q. Flagg, A. Savva, J. Surgailis, B. D. Paulsen, D. Moia, X. Chen, S. Griggs, J. T. Mefford, R. B. Rashid, A. Marks, S. Inal, D. S. Ginger, A. Giovannitti and J. Nelson, Reversible electrochemical charging of n-type conjugated polymer electrodes in aqueous electrolytes, *J. Am. Chem. Soc.*, 2021, **143**, 14795–14805.
42 A. Savva, C. Cendra, A. Giugni, B. Torre, J. Surgailis, D. Ohayon, A. Giovannitti, I. McCulloch, E. Di Fabrizio, A. Salleo, J. Rivnay and S. Inal, Influence of water on the performance of organic electrochemical transistors, *Chem. Mater.*, 2019, **31**, 927–937.
43 J. Duan, G. Zhu, L. Wang, J. Chen, S. Cong, X. Zhu, Y. Zhou, Z. Li, I. McCulloch and W. Yue, Highly Efficient Mixed Conduction in N-type Fused Small Molecule Semiconductors, *Adv. Funct. Mater.*, 2022, **32**, 2203937.
44 P. Li and T. Lei, Molecular design strategies for high-performance organic electrochemical transistors, *J. Polym. Sci.*, 2022, **60**, 377–392.
45 D. Rawlings, E. M. Thomas, R. A. Segalman and M. L. Chabinyc, Controlling the doping mechanism in poly(3-hexylthiophene) thin-film transistors with polymeric ionic liquid dielectrics, *Chem. Mater.*, 2019, **31**, 8820–8829.
46 F. Cicoira, M. Sessolo, O. Yaghmazadeh, J. A. DeFranco, S. Y. Yang and G. G. Malliaras, Influence of device

geometry on sensor characteristics of planar organic electrochemical transistors, *Adv. Mater.*, 2010, **22**, 1012–1016.
47 D. T. Simon, E. O. Gabrielsson, K. Tybrandt and M. Berggren, Organic bioelectronics: bridging the signaling gap between biology and technology, *Chem. Rev.*, 2016, **116**, 13009–13041.
48 C.-Y. Yang, M.-A. Stoeckel, T.-P. Ruoko, H.-Y. Wu, X. Liu, N. B. Kolhe, Z. Wu, Y. Puttisong, C. Musumeci, M. Massetti, H. Sun, K. Xu, D. Tu, W. M. Chen, H. Y. Woo, M. Fahlman, S. A. Jenekhe, M. Berggren and S. Fabiano, A high-conductivity n-type polymeric ink for printed electronics, *Nat. Commun.*, 2021, **12**, 2354.
49 A. Giovannitti, I. P. Maria, D. Hanifi, M. J. Donahue, D. Bryant, K. J. Barth, B. E. Makdah, A. Savva, D. Moia, M. Zetek, P. R. F. Barnes, O. G. Reid, S. Inal, G. Rumbles, G. G. Malliaras, J. Nelson, J. Rivnay and I. McCulloch, The role of the side chain on the performance of n-type conjugated polymers in aqueous electrolytes, *Chem. Mater.*, 2018, **30**, 2945–2953.
50 A. Paterson, N. Treat, W. Zhang, Z. Fei, G. Wyatt-Moon, H. Faber, G. Vourlias, P. Patsalas, O. Solomeshch, N. Tessler, M. Heeney and T. Anthopoulos, Small molecule/polymer blend organic transistors with hole mobility exceeding 13 $cm^2 V^{-1} s^{-1}$, *Adv. Mater.*, 2016, **28**, 7791–7798.
51 C. J. Kousseff, R. Halaksa, Z. S. Parr and C. B. Nielsen, Mixed ionic and electronic conduction in small-molecule semiconductors, *Chem. Rev.*, 2021, **122**, 4397–4419.
52 A. Facchetti, π-Conjugated polymers for organic electronics and photovoltaic cell applications, *Chem. Mater.*, 2011, **23**, 733–758.
53 J. T. Quinn, J. Zhu, X. Li, J. Wang and Y. Li, Recent progress in the development of n-type organic semiconductors for organic field effect transistors, *J. Mater. Chem. C*, 2017, **5**, 8654–8681.
54 S. Dai, Y. Chu, D. Liu, F. Cao, X. Wu, J. Zhou, B. Zhou, Y. Chen and J. Huang, Intrinsically ionic conductive cellulose nanopapers applied as all solid dielectrics for low voltage organic transistors, *Nat. Commun.*, 2018, **9**, 2737.
55 J. Jang, J. W. Kim, N. Park and J.-J. Kim, Air stable C60 based n-type organic field effect transistor using a perfluoropolymer insulator, *Org. Electron.*, 2008, **9**, 481–486.
56 J. Roncali, Molecular engineering of the band gap of π-conjugated systems: facing technological applications, *Macromol. Rapid Commun.*, 2007, **28**, 1761–1775.
57 Y. Li, P. Sonar, L. Murphy and W. Hong, High mobility diketopyrrolopyrrole (DPP)-based organic semiconductor materials for organic thin film transistors and photovoltaics, *Energy Environ. Sci.*, 2013, **6**, 1684–1710.
58 X. Yan, M. Xiong, J.-T. Li, S. Zhang, Z. Ahmad, Y. Lu, Z.-Y. Wang, Z.-F. Yao, J.-Y. Wang, X. Gu and T. Lei, Pyrazine-flanked diketopyrrolopyrrole (DPP): a new polymer building block for high-performance n-type organic thermoelectrics, *J. Am. Chem. Soc.*, 2019, **141**, 20215–20221.
59 Z. S. Parr, J. Borges-González, R. B. Rashid, K. J. Thorley, D. Meli, B. D. Paulsen, J. Strzalka, J. Rivnay and C. B. Nielsen, From p-to n-Type Mixed Conduction in Isoindigo-Based Polymers through Molecular Design, *Adv. Mater.*, 2022, **34**, 2107829.
60 K. Feng, W. Shan, S. Ma, Z. Wu, J. Chen, H. Guo, B. Liu, J. Wang, B. Li, H. Woo, S. Fabiano, W. Huang and X. Guo, Fused Bithiophene Imide Dimer-Based n-Type Polymers for High-Performance Organic Electrochemical Transistors, *Angew. Chem., Int. Ed.*, 2021, **133**, 24400–24407.
61 X. Chen, A. Marks, B. D. Paulsen, R. Wu, R. B. Rashid, H. Chen, M. Alsufyani, J. Rivnay and I. McCulloch, n-Type rigid semiconducting polymers bearing oligo (ethylene glycol) side chains for high-performance organic electrochemical transistors, *Angew. Chem., Int. Ed.*, 2021, **60**, 9368–9373.
62 H. Jia and T. Lei, Emerging research directions for n-type conjugated polymers, *J. Mater. Chem. C*, 2019, **7**, 12809–12821.
63 J. Chen, S. Cong, L. Wang, Y. Wang, L. Lan, C. Chen, Y. Zhou, Z. Li, I. McCulloch and W. Yue, Backbone coplanarity manipulation via hydrogen bonding to boost the n-type performance of polymeric mixed conductors operating in aqueous electrolyte, *Mater. Horiz.*, 2023, **10**, 607–618.
64 J. Shi, P. Li, X.-Y. Deng, J. Xu, Z. Huang, Y. Lei, Y. Wang, J.-Y. Wang, X. Gu and T. Lei, Revealing the role of polaron distribution on the performance of n-type organic electrochemical transistors, *Chem. Mater.*, 2022, **34**, 864–872.
65 M. Zhu, P. Li, J.-L. Li and T. Lei, Molecular packing and film morphology control in organic electrochemical transistors, *Mol. Syst. Des. Eng.*, 2022, **7**, 6–20.
66 J. Surgailis, A. Savva, V. Druet, B. D. Paulsen, R. Wu, A. Hamidi-Sakr, D. Ohayon, G. Nikiforidis, X. Chen and I. McCulloch, Mixed Conduction in an N-Type Organic Semiconductor in the Absence of Hydrophilic Side-Chains, *Adv. Funct. Mater.*, 2021, **31**, 2010165.
67 H. Y. Wu, C. Y. Yang, Q. Li, N. Kolhe, X. Strakosas, M.-A. Stoeckel, Z. Wu, W. Jin, M. Savvakis, R. Kroon, D. Tu, H. Woo, M. Berggren, S. Jenekhe and S. Fabiano, Influence of molecular weight on the organic electrochemical transistor performance of ladder-type conjugated polymers, *Adv. Mater.*, 2022, **34**, 2106235.
68 X. Guo, R. P. Ortiz, Y. Zheng, Y. Hu, Y.-Y. Noh, K.-J. Baeg, A. Facchetti and T. J. Marks, Bithiophene-Imide-Based Polymeric Semiconductors for Field-Effect Transistors: Synthesis, Structure–Property Correlations, Charge Carrier Polarity, and Device Stability, *J. Am. Chem. Soc.*, 2011, **133**, 1405–1418.
69 X. Wu, T. L. D. Tam, S. Chen, T. Salim, X. Zhao, Z. Zhou, M. Lin, J. Xu, Y. L. Loo and W. L. Leong, All-Polymer Bulk-Heterojunction Organic Electrochemical Transistors with Balanced Ionic and Electronic Transport, *Adv. Mater.*, 2022, **34**, 2206118.
70 J. Guo, L. Q. Flagg, D. K. Tran, S. E. Chen, R. Li, N. B. Kolhe, R. Giridharagopal, S. A. Jenekhe, L. J. Richter and D. S. Ginger, Hydration of a side-chain-free n-type semiconducting ladder polymer driven by electrochemical doping, *J. Am. Chem. Soc.*, 2023, **145**(3), 1866–1876.
71 D. Ohayon, L. Q. Flagg, A. Giugni, S. Wustoni, R. Li, T. C. Hidalgo Castillo, A.-H. Emwas, R. Sheelamanthula, I. McCulloch and L. J. Richter, Salts as additives: a route to

improve performance and stability of n-type organic electrochemical transistors, *ACS Mater. Au*, 2023, **3**(3), 242–254.

72 A. F. Paterson, H. Faber, A. Savva, G. Nikiforidis, M. Gedda, T. C. Hidalgo, X. Chen, I. McCulloch, T. D. Anthopoulos and S. Inal, On the role of contact resistance and electrode modification in organic electrochemical transistors, *Adv. Mater.*, 2019, **31**, 1902291.

73 M. Kawan, T. C. Hidalgo, W. Du, A.-M. Pappa, R. M. Owens, I. McCulloch and S. Inal, Monitoring supported lipid bilayers with n-type organic electrochemical transistors, *Mater. Horiz.*, 2020, **7**, 2348–2358.

74 I. Maria, B. Paulsen, A. Savva, D. Ohayon, R. Wu, R. Hallani, A. Basu, W. Du, T. Anthopoulos, S. Inal, J. Rivnay, I. McCulloch and A. Giovannitti, The effect of alkyl spacers on the mixed ionic-electronic conduction properties of n-type polymers, *Adv. Funct. Mater.*, 2021, **31**, 2008718.

75 D. Ohayon, A. Savva, W. Du, B. D. Paulsen, I. Uguz, R. S. Ashraf, J. Rivnay, I. McCulloch and S. Inal, Influence of side chains on the n-type organic electrochemical transistor performance, *ACS Appl. Mater. Interfaces*, 2021, **13**, 4253–4266.

76 D. Jeong, I. Y. Jo, S. Lee, J. H. Kim, Y. Kim, D. Kim, J. R. Reynolds, M. H. Yoon and B. J. Kim, High-performance n-type organic electrochemical transistors enabled by aqueous solution processing of amphiphilicity-driven polymer assembly, *Adv. Funct. Mater.*, 2022, **32**, 2111950.

77 S. Cong, J. Chen, L. Wang, L. Lan, Y. Wang, H. Dai, H. Liao, Y. Zhou, Y. Yu, J. Duan, Z. Li, I. McCulloch and W. Yue, Donor functionalization tuning the n-type performance of donor–acceptor copolymers for aqueous-based electrochemical devices, *Adv. Funct. Mater.*, 2022, **32**, 2201821.

78 H. Jia, Z. Huang, P. Li, S. Zhang, Y. Wang, J.-Y. Wang, X. Gu and T. Lei, Engineering donor–acceptor conjugated polymers for high-performance and fast-response organic electrochemical transistors, *J. Mater. Chem. C*, 2021, **9**, 4927–4934.

79 I. P. Maria, S. Griggs, R. B. Rashid, B. D. Paulsen, J. Surgailis, K. Thorley, V. N. Le, G. T. Harrison, C. Combe, R. Hallani, A. Giovannitti, A. F. Paterson, S. Inal, J. Rivnay and I. McCulloch, Enhancing the backbone coplanarity of n-type copolymers for higher electron mobility and stability in organic electrochemical transistors, *Chem. Mater.*, 2022, **34**, 8593–8602.

80 K. Feng, W. Shan, J. Wang, J. W. Lee, W. Yang, W. Wu, Y. Wang, B. J. Kim, X. Guo and H. Guo, Cyano-Functionalized n-Type Polymer with High Electron Mobility for High-Performance Organic Electrochemical Transistors, *Adv. Mater.*, 2022, **34**, 2201340.

81 A. Erhardt, A. Hochgesang, C. R. McNeill and M. Thelakkat, A Competitive n-Type OECT Material via Copolymerization of Electron Deficient Building Blocks, *Adv. Electron. Mater.*, 2023, 2300026.

82 Y. Wang, E. Zeglio, L. Wang, S. Cong, G. Zhu, H. Liao, J. Duan, Y. Zhou, Z. Li, D. Mawad, A. Herland, W. Yue and I. McCulloch, Green Synthesis of Lactone-Based Conjugated Polymers for n-Type Organic Electrochemical Transistors, *Adv. Funct. Mater.*, 2022, **32**, 2111439.

83 H. Liao, J. Chen, L. Lan, Y. Yu, G. Zhu, J. Duan, X. Zhu, H. Dai, M. Xiao, Z. Li, W. Yue and I. McCulloch, Efficient n-type small-molecule mixed ion-electron conductors and application in hydrogen peroxide sensors, *ACS Appl. Mater. Interfaces*, 2022, **14**, 16477–16486.

84 C. G. Bischak, L. Q. Flagg, K. Yan, C.-Z. Li and D. S. Ginger, Fullerene active layers for n-type organic electrochemical transistors, *ACS Appl. Mater. Interfaces*, 2019, **11**, 28138–28144.

85 G. Zhu, J. Chen, J. Duan, H. Liao, X. Zhu, Z. Li, I. McCulloch and W. Yue, Fluorinated Alcohol-Processed N-Type Organic Electrochemical Transistor with High Performance and Enhanced Stability, *ACS Appl. Mater. Interfaces*, 2022, **14**, 43586–43596.

86 J. Duan, G. Zhu, L. Lan, J. Chen, X. Zhu, C. Chen, Y. Yu, H. Liao, Z. Li, I. McCulloch and W. Yue, Electron-Deficient Polycyclic Molecules via Ring Fusion for n-Type Organic Electrochemical Transistors, *Angew. Chem. Int. Ed.*, 2023, **62**, e202213737.

87 J. Duan, G. Zhu, J. Chen, C. Zhang, X. Zhu, H. Liao, Z. Li, H. Hu, I. McCulloch, C. B. Nielsen and W. Yue, Highly Efficient Mixed Conduction in a Fused Oligomer n-Type Organic Semiconductor Enabled by 3D Transport Pathways, *Adv. Mater.*, 2023, **35**, e2300252.

88 S. G. Higgins, A. Lo Fiego, I. Patrick, A. Creamer and M. M. Stevens, Organic bioelectronics: using highly conjugated polymers to interface with biomolecules, cells, and tissues in the human body, *Adv. Mater. Technol.*, 2020, **5**, 2000384.

89 Y. Zhang, G. Ye, T. Pol, J. Dong, E. van Doremaele, I. Krauhausen, Y. Liu, P. Gkoupidenis, G. Portale, J. Song, R. Chiechi and Y. Van, de Burgt, High-performance organic electrochemical transistors and neuromorphic devices comprising naphthalenediimide-dialkoxybithiazole copolymers bearing glycol ether pendant groups, *Adv. Funct. Mater.*, 2022, **32**, 2201593.

90 S. Zhang, M. Massetti, T.-P. Ruoko, D. Tu, C. Y. Yang, X. Liu, Z. Wu, Y. Lee, R. Kroon, P. Persson, H. Woo, M. Berggren, C. Müller, M. Fahlman and S. Fabiano, Synergistic Effect of Multi-Walled Carbon Nanotubes and Ladder-Type Conjugated Polymers on the Performance of N-Type Organic Electrochemical Transistors, *Adv. Funct. Mater.*, 2022, **32**, 2106447.

91 K. Feng, H. Guo, H. Sun and X. Guo, n-Type Organic and Polymeric Semiconductors Based on Bithiophene Imide Derivatives, *Acc. Chem. Res.*, 2021, **54**, 3804–3817.

92 X. Zou, S. Cui, J. Li, X. Wei and M. Zheng, Diketopyrrolopyrrole based organic semiconductor materials for field-effect transistors, *Front. Chem.*, 2021, **9**, 671294.

93 T. Lei, J.-Y. Wang and J. Pei, Design, synthesis, and structure–property relationships of isoindigo-based conjugated polymers, *Acc. Chem. Res.*, 2014, **47**, 1117–1126.

94 A. Onwubiko, W. Yue, C. Jellett, M. Xiao, H.-Y. Chen, M. K. Ravva, D. A. Hanifi, A.-C. Knall, B. Purushothaman, M. Nikolka, J.-C. Flores, A. Salleo, J.-L. Bredas, H. Sirringhaus, P. Hayoz and I. McCulloch, Fused electron deficient semiconducting polymers for air stable electron transport, *Nat. Commun.*, 2018, **9**, 416.

95 M. Xie, H. Liu, M. Wu, C. Chen, J. Wen, L. Bai, J. Yu and W. Huang, Cycling stability of organic electrochemical transistors, *Org. Electron.*, 2023, 106777.
96 A. F. Paterson, A. Savva, S. Wustoni, L. Tsetseris, B. D. Paulsen, H. Faber, A. H. Emwas, X. Chen, G. Nikiforidis, T. C. Hidalgo, M. Moser, I. P. Maria, J. Rivnay, I. McCulloch, T. D. Anthopoulos and S. Inal, Water stable molecular n-doping produces organic electrochemical transistors with high transconductance and record stability, *Nat. Commun.*, 2020, **11**, 3004.
97 C. Y. Yang, D. Tu, T.-P. Ruoko, J. Gerasimov, H. Y. Wu, P. C. Harikesh, M. Massetti, M.-A. Stoeckel, R. Kroon, C. Müller, M. Berggren and S. Fabiano, Low-Power/High-Gain Flexible Complementary Circuits Based on Printed Organic Electrochemical Transistors, *Adv. Electron. Mater.*, 2022, **8**, 2100907.
98 Z. Xie, C. Zhuge, Y. Zhao, W. Xiao, Y. Fu, D. Yang, S. Zhang, Y. Li, Q. Wang, Y. Wang, W. Yue and I. McCulloch, All-Solid-State Vertical Three-Terminal N-Type Organic Synaptic Devices for Neuromorphic Computing, *Adv. Funct. Mater.*, 2022, **32**, 2107314.
99 C. Reese, M. Roberts, M.-M. Ling and Z. Bao, Organic thin film transistors, *Mater. Today*, 2004, **7**, 20–27.
100 X. Zhao and X. Zhan, Electron transporting semiconducting polymers in organic electronics, *Chem. Soc. Rev.*, 2011, **40**, 3728–3743.
101 T. Leydecker, Z. M. Wang, F. Torricelli and E. Orgiu, Organic-based inverters: basic concepts, materials, novel architectures and applications, *Chem. Soc. Rev.*, 2020, **49**, 7627–7670.
102 J. R. Hauser, Noise margin criteria for digital logic circuits, *IEEE Trans. Educ.*, 1993, **36**, 363–368.
103 M. Sessolo, J. Rivnay, E. Bandiello, G. G. Malliaras and H. J. Bolink, Ion-selective organic electrochemical transistors, *Adv. Mater.*, 2014, **26**, 4803–4807.
104 S. Wustoni, C. Combe, D. Ohayon, M. H. Akhtar, I. McCulloch and S. Inal, Membrane-Free Detection of Metal Cations with an Organic Electrochemical Transistor, *Adv. Funct. Mater.*, 2019, **29**, 1904403.
105 H. L. Park, Y. Lee, N. Kim, D. G. Seo, G. T. Go and T. W. Lee, Flexible Neuromorphic Electronics for Computing, Soft Robotics, and Neuroprosthetics, *Adv. Mater.*, 2020, **32**, e1903558.
106 J. Liao, H. Si, X. Zhang and S. Lin, Functional sensing interfaces of PEDOT: PSS organic electrochemical transistors for chemical and biological sensors: a mini review, *Sensors*, 2019, **19**, 218.
107 Y. Liang, A. Offenhäusser, S. Ingebrandt and D. Mayer, PEDOT:PSS-based bioelectronic devices for recording and modulation of electrophysiological and biochemical cell signals, *Adv. Healthcare Mater*, 2021, **10**, 2100061.
108 H. Shi, C. Liu, Q. Jiang and J. Xu, Effective approaches to improve the electrical conductivity of PEDOT:PSS: a review, *Adv. Electron. Mater.*, 2015, **1**, 1500017.
109 S. Griggs, A. Marks, D. Meli, G. Rebetez, O. Bardagot, B. D. Paulsen, H. Chen, K. Weaver, M. I. Nugraha and E. A. Schafer, The effect of residual palladium on the performance of organic electrochemical transistors, *Nat. Commun.*, 2022, **13**, 7964.
110 G. A. Woods, N. J. Rommelfanger and G. Hong, Bioinspired materials for in vivo bioelectronic neural interfaces, *Matter*, 2020, **3**, 1087–1113.

